IEEE MICROWAVE MAGAZINE – Vol. 23(4) – pp. 24-44

Flexible Electronics for Wireless Communication: A Technology and Circuit Design Review With an Application Example

Tilo Meister, *Member, IEEE,* Koichi Ishida, *Member, IEEE,* Corrado Carta, *Senior Member, IEEE,* Niko Münzenrieder, *Senior Member, IEEE,* Frank Ellinger, *Senior Member, IEEE*

***Abstract*—This article reviews the current state of the art of wireless communication in fully flexible electronics technologies. Modern flexible electronics technologies allow the fabrication of devices that integrate in our daily lives in a very natural way. They can be incredibly light weight and transparent to the point of being virtually unperceivable. The combination of this subtlety with the ability to communicate wirelessly, plus the infrastructure established for the internet-of-things, might lead to a whole new class of flexible devices that are omnipresent in our lives.**

This article first gives an overview of flexible organic, metal-oxide, carbon-based, amorphous-silicon-based, and monolithic-silicon-based technologies. After that, key circuits that are needed for wireless communication systems and aspects of their realization are discussed. The discussion of circuits and applications is focused around the favorable flexible metal-oxide thin-film technologies.

Finally, as an application example, a next-generation flexible wireless moisture sensor from the authors' recent work and details about its circuit block are presented. The moisture sensor tag is fully integrated in a 5 V flexible amorphous indium gallium zinc oxide (a-IGZO) TFT technology. The tag consists of an on-off-keying (OOK) modulator with digitally controlled oscillator (DCO), a moisture sensor, a pseudo-CMOS clocked comparator, a latch, a low frequency oscillator, and an antenna. The wireless moisture sensor is fabricated on a plastic substrate and characterized with a 5 V supply voltage. The integrated DCO synthesizes the carrier frequency on-chip. Its average frequency of oscillation is 1.36 MHz, and it achieves a tuning range of 15 %. The OOK-modulator successfully modulates a $\leq$ 50 kHz baseband signal with a 300 mV maximum output swing and a modulation index of around 50 %. The clocked comparator achieves 28 dB open loop gain with a minimum input offset of 25 mV. The moisture sensor is characterized with a small drop of tap water. The water drop covering the sensor area of 0.44 mm^2 raises the sensor output from 0.28 mV to 1.60 V, which is detected by the comparator and fed to the OOK-modulator by the latch.

I. Introduction

There is a practical gap between conventional rigid electronics and bendable items from daily-life, such as paper, tape, textiles, and the human body. This space can be bridged by flexible transistor technologies, which typically offer bendability, a light weight, ultrathin dimensions, transparency, sometimes stretchability, suitability for large areas, and a low cost. Thanks to the continuous increase of the maximal operation frequency of flexible electronics, wireless communication is becoming one of the promising enablers for many new applications and is widely studied.

T. Meister, K. Ishida, C. Carta, and F. Ellinger are with the Chair of Circuit Design and Network Theory, Technische Universität Dresden, 01069 Dresden, Germany (e-mail: tilo@ieee.org). F. Ellinger is also with the Centre for Tactile Internet with Human-in-the-Loop (CeTI). N. Münzenrieder is with the Free University of Bolzano, Bozen-Bolzano, Italy.

Manuscript published March 2nd 2022.
Digital Object Identifier 10.1109/MMM.2021.3136684

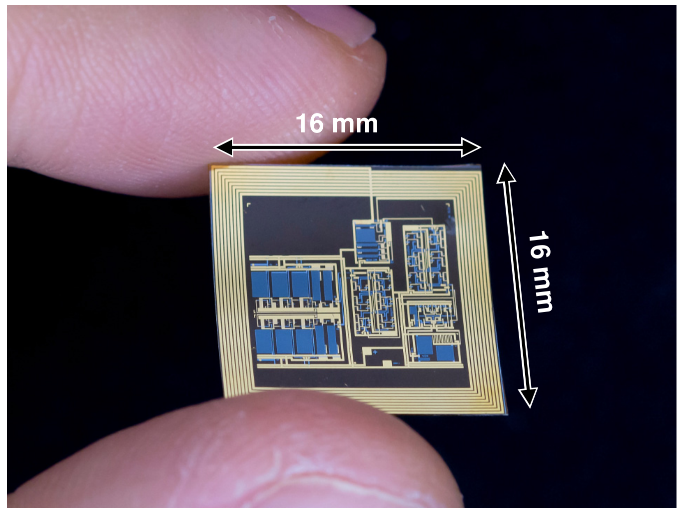

Fig. 1. Prototype of a fully flexible, fully integrated moisture sensor with on-off keying (OOK) transmitter on a 50 µm polyimide substrate. It has an area of $16 \times 16\,\mathrm{mm}^2$ and includes a moisture sensor, sensor readout circuitry, two local oscillators, an OOK modulator, and an antenna.

For a long time, electronics have advanced in terms of speed, power consumption, integration density, and cost. In particular, reductions in feature sizes, which lead to improvements in integration density, are expected to keep slowing down, e.g. due to thermal noise constraints. This trend has long been predicted, and it has motivated the investigation of multiple alternative electronic technologies, including mechanically flexible ones.

Figure 1 displays an advanced fully flexible moisture sensor, which was designed by the authors and is presented as an application example in Section V. It can wirelessly transmit a sensor value via its integrated transmitter. It was manufactured on a 50 µm-thick polyimide substrate, using a 5 V flexible technology [1], [2] based on the metal-oxide (MO) semiconductor indium gallium zinc oxide (IGZO). A key characteristic is that this technology can be fabricated at temperatures sufficiently low that the polyimide substrate is not damaged.

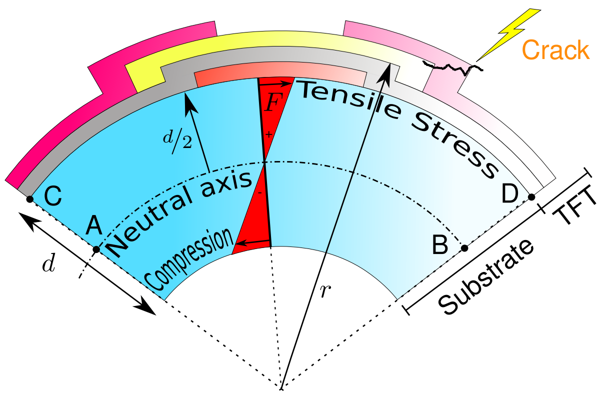

Fig. 2. Compressive and tensile stress in a bent thin-film transistor (TFT) circuit. The red markers in the substrate cross-section qualify the amount of stress in the circuit.

The fully integrated tag consists of an on-off-keying (OOK) modulator with a digitally controlled oscillator (DCO), a moisture sensor, a pseudo-CMOS clocked comparator, a latch, a low-frequency oscillator, and an antenna. The integrated DCO synthesizes the carrier frequency on-chip. Its average frequency of oscillation is 1.36 MHz, and it achieves a tuning range of 15 %. The OOK modulator successfully modulates a ≤ 50 kHz baseband signal, with a 300 mV maximum output swing and a modulation index of around 50 %. The clocked comparator achieves 28 dB open-loop gain with a minimum input offset of 25 mV.

In general, any conductor, any semiconductor, any insulator, any composite of those, or any solid material is bendable to some degree. The limit for bending any solid, which is called the minimum bending radius $r_{\min}$, can be expressed in terms of the material's maximum tensile strain ϵ_{yield} and thickness d. Figure 2 illustrates the compressive and tensile strain in a cross-section of a bent thin-film transistor (TFT) circuit. The peak tensile and compressive strains occur on the upper and lower surfaces, respectively. The tensile strain is the ratio of the solid's unstressed length $L_0 = \overline{\mathsf{AB}}$ and the amount of its elongation $\Delta L = \overline{\mathsf{CD}} - \overline{\mathsf{AB}}$. It is usually given as percentage:

$$\epsilon = \frac{\Delta L}{L_0}. \tag{1}$$

Tensile strain ϵ can be related to tensile stress σ by Young's modulus E:

$$E \equiv \frac{\text{tensile stress}}{\text{tensile strain}} = \frac{\sigma}{\epsilon} = \frac{F/A}{\Delta L/L_0}, \tag{2}$$

where A and F are the cross-sectional area and the perpendicular force applied to it, respectively.

The substrates used for flexible electronics are often around 10 µm to 50 µm thick, and can be as thin as 1.2 µm. The active layers of a TFT circuit and interconnect layers tend to accumulate to a thickness of roughly 1 µm or less. On top of the active layers, there can be a thick passivation, or protective, layer.

If the cumulative thickness of the active TFT layers and passivation is on the order of the substrate thickness, all layers have a noticeable effect on the position of the neutral axis, which is the axis without any strain. In this case, all layers have to be carefully considered when determining the distance $d/2$ between the neutral axis and the layer to be considered. With careful design, this can enable an active TFT layer to be located at or close to the neutral axis, which minimizes strain while maximizing bendability. For thick homogeneous substrates, however, the neutral axis can be estimated to be at the center of the substrate, and $d/2$ can be approximated to be half the substrate thickness. From this simplification and the relations shown in Fig. 2, the tensile strain in the TFT layers due to bending can be calculated as

$$\epsilon = \frac{\Delta L}{L_0} = \frac{d}{2} \cdot \frac{1}{r}. \tag{3}$$

The maximum strain ϵ_{yield} of each material before it yields can be determined from mechanical measurements. Thus, the minimum bending radius $r_{\min}$ of a TFT circuit before a certain layer fails due to deformation, kinking, or cracking can be calculated:

$$r_{\min} = \frac{d}{2 \cdot \epsilon_{\text{yield}}}. \tag{4}$$

As evident from Eq. (4), the thinner a solid gets $d\downarrow$, the tighter it can be bent $r_{\min}\downarrow$ before deforming, kinking, or rupturing. Consequently, the active layers of flexible electronics always have to be close to the neutral axis of the substrate or package. This can be achieved by using thin substrates and by sandwiching the active layers in the middle of a flexible package.

For thin films of a typical conductor, such as gold and copper, ϵ_{yield} is between only 1 % and 2 % [3]. Such a thin gold trace on the surface of a 50 µm thick polyimide substrate would start to crack at a bending radius of $r \approx 2.5$ mm, while a copper film on a 775 µm thick silicon (Si) die would theoretically start to crack at a bending radius of $r \approx 40$ mm. This is, however, a theoretical value, because at a ten times larger radius [4], the silicon substrate would already have started to crack.

II. Flexible Technologies

At the heart of fully flexible electronic systems are fully bendable integrated circuits (ICs). The mobility μ of the semiconductor(s) and the transit frequency f_t of the transistor devices are central figures of merit to evaluate the performance of the flexible IC.

Mobility is a measure of how well carriers are transported in a material and differs for holes and electrons. It is, among other things, a figure of merit for semiconductor layers. This mobility often does not consider effects such as contact resistance. Mobility can be defined and measured in different ways and their different values can differ significantly. The effective saturation mobility μ_{eff} is a particularly useful definition for circuit designers. It serves as a figure of merit for the charge transport efficiency, including the effects of a transistor's source contact and drain contact interface:

$$\mu_{\text{eff}} = \frac{2L}{WC_{ox}} \frac{d^2 I_{D,sat}}{dV_{GS}^2}, \tag{5}$$

where L is the channel length, W is the channel width, C_{ox} is the specific gate capacitance, V_{GS} is the gate-source voltage, and $I_{D,sat}$ is the drain current in the saturation regime.

The transit frequency f_t of a TFT is a second figure of merit for its performance. In extension of μ_{eff}, it includes all parasitics of the TFT device, such as the gate capacitance and the gate, source, and drain resistances. The transit frequency is where the short circuit gain h_{21} drops to unity. It can be expressed in terms of the TFT's transconductance g_m and gate capacitance C_G:

$$f_t = \frac{g_m}{2\pi C_G}. \tag{6}$$

The ring oscillator stage delay τ, which can be calculated from a ring oscillator's frequency of oscillation f_{osc} (see Section III-C), is a figure of merit that includes TFT device and chip level parasitics, such as interconnect. This is discussed in the following.

Wireless applications require fast devices, because antennas are prohibitively large at lower frequencies. High-speed transistor devices alone, however, are not sufficient to make flexible devices for actual applications. A whole ecosystem of compatible flexible components is required. Systems and devices usually require flexible power supplies, sensors, buttons, displays, antennas, and packaging. Figure 3 provides examples of flexible components in one compatible ecosystem [5], [6]. This overview also illustrates how flexible electronics require highly interdisciplinary research, especially in the domains of physics, chemistry, material science, electronics, and engineering in general.

Today, flexible devices can be realized in a number of ways. Among other things, they differ in the required process temperatures and thus in the compatible substrates. For example, only few types of printed electronics can be fabricated on a piece of paper, since paper is not stable at higher processing temperatures and because it has a very rough surface. Polyimide is a popular substrate for printed as well as for vacuum-processed flexible electronics, because of its smooth surface and relatively good temperature stability up to around 230°C.

The main categories of flexible electronics are compared in Table I, and their primary characteristics are discussed in the following sections.

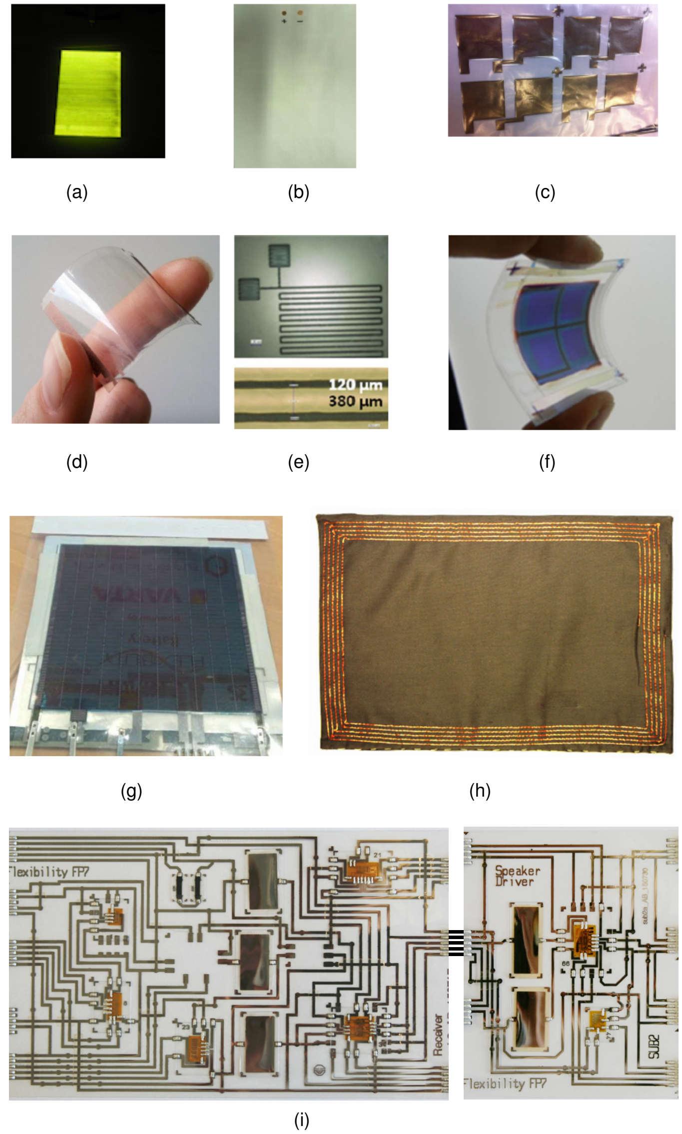

Fig. 3. Examples of flexible devices and sensors of a flexible ecosystem: (a) a 6 cm^2 organic LED, (b) a 24 V disposable battery, (c) a 24 V rechargeable battery, (d) a 5 cm^2 piezoelectric speaker, (e) a resistive temperature sensor, (f) a 2×2 array of organic photodiodes for motion detection on two axes, (g) solar power module stacked with a flexible printed nickel-metal hydride (NiMH) rechargeable battery and an organic photovoltaic device (OPV), (h) a textile antenna with copper wires woven into the fabric, and (i) an inkjet printed circuit board based on a polyethylene terephthalate (PET) substrate. [5], [6] (a) – (f) © 2013 IEEE. Reproduced, with permission, from [5]. (g) – (i) © 2016 IEEE. Reproduced, with permission, from [6].

A. Conventional Rigid Components on Flexible PCB

The technology mentioned in this subsection is not a flexible electronics technology, but rather a flexible packaging technology. Yet, it still deserves a mention in the context of this article, because of its maturity, cost efficiency, and usefulness for many practical applications.

Conventional rigid integrated circuits and electronic components can be so small, that from a macro-perspective they can be used to make devices that appear to be flexible. This can be achieved by using flexible packaging and flexible printed circuit board technologies. The technology of flexible printed circuit boards [7], [8] is very affordable and has been available for many years. It is based on a stack of polyimide, copper, and adhesive layers. It is readily available with 1 to 4 copper interconnect layers. It can be ordered in different thicknesses, which cover different application and bendability requirements. In its standard configuration, a 1 layer flexPCB has a thickness of around 93 µm. A standard 4 layer configuration is around 285 µm thick. Standard electronics components can be soldered to a flexPCB. The result are semi-flexible electronics that are bendable in certain areas, while being stiff in relatively small areas around the rigid components. This technology can obviously achieve very high performance and is frequently used for highly compact 3D integration, for example in photo cameras. However, such a flexPCB has to be relatively large and is not very reliable when being

TABLE I
COMPARISON OF FLEXIBLE ELECTRONICS TECHNOLOGIES.

	Organic TFT	**Metal-Oxide TFT**	**Carbon TFT**	**a-Si:H TFT**	**LTPS TFT**	**Thinned Si Transistor**
Technology Readiness	-	+	- -	++	+/-	++
Suitable for RF Application	+/-	+	++	-	+	++
Cost / Complexity	++	+	+	+	+/-	- -
Substrates	paper, plastics	plastics	plastics	polyimide	polyimide	silicon
Types	p-type, (n-type)	n-type, (p-type)	p-type, n-type, ambipolar	n-type, p-type	n-type, p-type	n-type, p-type
Mobility n-Type Device	$2\,\mathrm{cm^2/(V{\cdot}s)}$	$75\,\mathrm{cm^2/(V{\cdot}s)}$	$50\,\mathrm{cm^2/(V{\cdot}s)}$	$1\,\mathrm{cm^2/(V{\cdot}s)}$	$200\,\mathrm{cm^2/(V{\cdot}s)}$	$400\,\mathrm{cm^2/(V{\cdot}s)}$
Mobility p-Type Device	$5\,\mathrm{cm^2/(V{\cdot}s)}$	$0.5\,\mathrm{cm^2/(V{\cdot}s)}$	$150\,\mathrm{cm^2/(V{\cdot}s)}$	$0.1\,\mathrm{cm^2/(V{\cdot}s)}$	$100\,\mathrm{cm^2/(V{\cdot}s)}$	$100\,\mathrm{cm^2/(V{\cdot}s)}$
Mobility Ambipolar Device			$120\,\mathrm{cm^2/(V{\cdot}s)}$			
Transit Frequency	40 MHz	2.1 GHz (typ. 100 MHz)		1 MHz	100 MHz	≥ 100 GHz
Electrical Stability	- -	+/-	+	+	+	++
Mechanical Durability	+	+	+	-	-	+
Channel Scalability	+/-	+	++	+	-	++

bent repeatedly, because very high local stress is induced in the solder joints and substrate areas adjacent to the stiff components. To mitigate this, flexPCBs can be re-enforced locally, which however reduces bendability.

B. Flexible Organic TFTs

Organic semiconductors can be deposited and structured on rigid and flexible substrates through thin and thick-film methods. A variety of semiconducting materials is studied today. P-type materials perform best [9]. N-type materials are also possible and widle researched [10], [11]. In organic technologies, field-effect transistors as well as heterojunction transistors can be made. The most popular and fast p-type organic semiconductors are pentacene [12] and rubrene [9], which are not stable in air. One very popular n-type organic semiconductor is fulleren C_{60} [12], [13].

In combination with compatible conductive and dielectric materials, which are not necessarily truly organic, circuits can be integrated. Thick-film technologies, in particular, are compatible with many substrates. Most often, plastic films and paper are used. A drawback of organic electronics is that they tend to require large supply voltages. Tens of volts is not uncommon as supply voltage for organic circuits [14], [15]. Effective carrier mobilities in the range of $5\,\mathrm{cm^2/(V{\cdot}s)}$ and transistor transit frequencies up to 40 MHz are reported in the literature [9], [13].

Before organic circuits will achieve wider use, organic semiconductors' speed, stability in air, and required supply voltages have to be improved.

C. Flexible Metal-Oxide and Metal-Chalcogenide TFTs

Certain metal-oxides (MOs), metal-chalcogenides, and their alloys behave like semiconductors and can be deposited by thin-film technologies. The most prominent examples are indium gallium zinc oxide (IGZO), indium tin oxide (ITO), indium zinc oxide (IZO), and molybdenum disulfide (MoS2). Among the compatible flexible substrates are temperature stable plastic films, such as polyimide. The substrates have to provide a good tradeoff between temperature stability and elasticity. In general, semiconductor performance in this class can be improved by increasing the annealing temperatures, which is primarily limited by the stability of the substrate that is used. Effective carrier mobilities up to $76.8\,\mathrm{cm^2/Vs}$ and transistor transit frequencies up to 2.1 GHz have been reported for flexible polyimide films [16], [17]. P-type MO-semiconductors, including nickel oxide (NiO), exist but have inferior performance [18]. Therefore, MO-TFT technologies are considered to be n-type only. The combination of MO-TFTs with organic technologies, amorphous silicon (a-Si) technologies, and carbon nanotube (CNT) based technologies is the subject of research [19], [20] to develop hybrid-CMOS technologies.

Among flexible electronics technologies, MO-technologies provide the most promising compromise among speed, availability, and cost for wireless communication.

D. Flexible Carbon Allotrope and Carbon Nanowire TFTs

Some carbon allotropes and carbon nanowires can have semiconducting properties. Buying ready-made and highly pure solutions of semiconducting allotropes and nanowires has been possible for several years. Still, structuring transistor devices from these materials remains very challenging. The footprint of carbon-based transistor devices is usually very small. The carrier mobilities in rigid carbon nanotubes $100{,}000\,\mathrm{cm^2/(V{\cdot}s)}$ and graphene $200{,}000\,\mathrm{cm^2/(V{\cdot}s)}$ exceed that of crystalline silicon $1{,}400\,\mathrm{cm^2/(V{\cdot}s)}$ by far. Graphene based TFTs, however, significantly fall behind these very high carrier mobilities reaching roughly $20{,}000\,\mathrm{cm^2/(V{\cdot}s)}$ [21]. Note that the effective mobility of graphene based TFTs, e.g. $116\,\mathrm{cm^2/(V{\cdot}s)}$ [22], is much lower than their carrier mobility.

Current TFTs based on carbon nanotubes (CNTs) also lag behind their ideal values and achieve an effective mobility $\leq 150\,\mathrm{cm}^2/(\mathrm{V{\cdot}s})$ [23]. If the effective mobilities of CNT- and graphene-based TFTs can be improved toward the values promised by their pure base materials, transit frequencies in the high gigahertz-range can be expected.

E. Flexible Silicon TFTs

Flexible TFTs can be made from thin films of amorphous silicon (a-Si), hydrogenated amorphous silicon (a-Si:H), polysilicon (poly-Si), nanocrystaline silicon (nc-Si), and low-temperature polycrystalline silicon (LTPS). These technologies can provide n-type as well as p-type devices, and CMOS circuits are possible. They are mature and available in consumer electronic products, mainly on rigid substrates [24]. Their major commercial application lies in active-matrix liquid crystal displays (AMLCDs). All of them are, with reduced performance, reduced uniformity, and reduced scalability, compatible with flexible substrates. Among them, a-Si is the slowest with carrier mobilities around $0.5\,\mathrm{cm}^2/(\mathrm{V{\cdot}s})$ [25]; a-Si:H has reportedly shown mobilities in the range of $1.0\,\mathrm{cm}^2/(\mathrm{V{\cdot}s})$ [26], [27]; nc-Si has been reported to achieve a mobility of $18\,\mathrm{cm}^2/(\mathrm{V{\cdot}s})$ [28]; and LTPS, which is the latest and fastest Si-TFT technology, achieves mobilities in the range of $50 - 100\,\mathrm{cm}^2/(\mathrm{V{\cdot}s})$ [29]. Technologies using a-Si and a-Si:H can have a good stability [30]. LTPS technologies are relatively complex, cannot be scaled well, and lack uniformity across large areas when compared to a-Si TFTs and MO-TFTs [31]–[33].

F. Flexible Thinned Monocrystalline Silicon Transistors

Conventional integrated silicon circuits are flexible after they have been thinned to a few tens of micrometers [34]. This category of flexible electronics benefits from the vast experience gained in the past decades. However, the handling, thinning, packaging, and modeling of the transistor characteristics are still challenging and require further research. Modeling these devices is challenging, because during thinning, the transistor characteristics may significantly change. Effective mobilities are in the range of $400\,\mathrm{cm}^2/(\mathrm{V{\cdot}s})$ to $800\,\mathrm{cm}^2/(\mathrm{V{\cdot}s})$ for n-type transistors and in the range of $100\,\mathrm{cm}^2/(\mathrm{V{\cdot}s})$ to $200\,\mathrm{cm}^2/(\mathrm{V{\cdot}s})$ for p-type transistors. Reported transit frequencies f_t exceed 100 GHz. Among fully flexible technologies, this is the most mature and fastest. However, it is by far the most complex and expensive one.

G. Device Cross-Sections

The transistor cross-section and layout are crucial for device performance, because they influence many characteristics. Figure 4 shows different cross-sections of TFTs that are studied and used. Figure 5 illustrates the dominant parasitics and their rough origins in a cross-section.

One major parasitic stems from the capacitances $\mathrm{C_{GS}}$ and $\mathrm{C_{GD}}$ that are mainly caused by the overlap L_D of the gate and the source/drain metals. These parasitic gate capacitances have to be minimized by minimizing L_D, which can be achieved through advanced lithography. Unfortunately, reducing L_D can also degrade device performance, because it increases the parasitic contact interface resistances $\mathrm{R_{cS}}$ and $\mathrm{R_{cD}}$. Consequently, an optimized tradeoff has to be found. Metal electrode resistances $\mathrm{R_S}$, $\mathrm{R_D}$, and $\mathrm{R_G}$ can be improved by using wider and thicker metals; however, this can impact other circuit and device characteristics, such as interconnect capacitances, bendability, and mechanical stability.

The cross-sections in Fig. 4 are all relevant to device performance optimization. The different orders of layers come with varying layer interfaces. Depositing a gold drain contact on top of an IGZO layer (staggered drain contact, Figs. 4 (a) and 4 (d)) does not result in the same interface characteristics as depositing an IGZO layer on top of a gold drain contact (coplanar drain contact, Fig. 4 (b) and 4 (e)). Therefore, changing the layer sequence will improve or degrade for example $\mathrm{R_{cD}}$.

Using two gates in a split configuration Fig. 4 (c) provides electrical control over the contact region and can improve performance. Using two gates in a double-gate configuration Fig. 4 (f) can improve the performance of the channel material.

The channel length is usually defined by lithography and can be reliably structured down to about 0.5 µm in MO-TFTs. A special case in this regard is the quasi-vertical TFT structure in Fig. 4 (h). TFTs with this cross-section can be fabricated with extremely short and precise channel lengths, because the channel length is defined by the thickness of a spacing layer, which can be controlled much better than the lateral dimensions resulting from an etching step. Achieving similarly short, repeatable, and precise channel lengths with the cross-section in Fig. 4 (a) requires structuring methods that are much more expensive and timeconsuming than lithography. For example, focused ion beam (FIB) etching can be used with the cross-section in Fig. 4 (a) to structure a channel with lengths down to 160 nm [42].

The truly vertical TFT structure in Fig. 4 (g) is mostly specific to organic TFTs and graphene-based hetero-junction TFTs. It enables the use of very thin and consistent layers in the channel.

Figure 6 provides a top view of a bottom-gate TFT (refer to Fig. 4 (a)).

H. Transistor Performance

Tables II and III detail a selection of transit frequencies and mobilities that have been reported in the literature for organic, metal-oxide, amorphous silicon, and carbon-based TFT transistor devices.

The tables show that devices made from the same semiconductor can greatly vary in performance. This is obviously due to the huge number of process parameters as well as different device geometries. The fastest organic transistor has an f_t of 40 MHz [13], which is not sufficient to build an amplifier at 13.56 MHz. As a rule of thumb, f_t should be ten times larger than the target frequency of operation. Consequently, organic transistors cannot be used to improve the wireless communication range of active RFID- and NFC-tags.

Metal-oxide TFTs with a transit frequency f_t of 135 MHz for IGZO and 2.1 GHz for ITO have been reported [17],

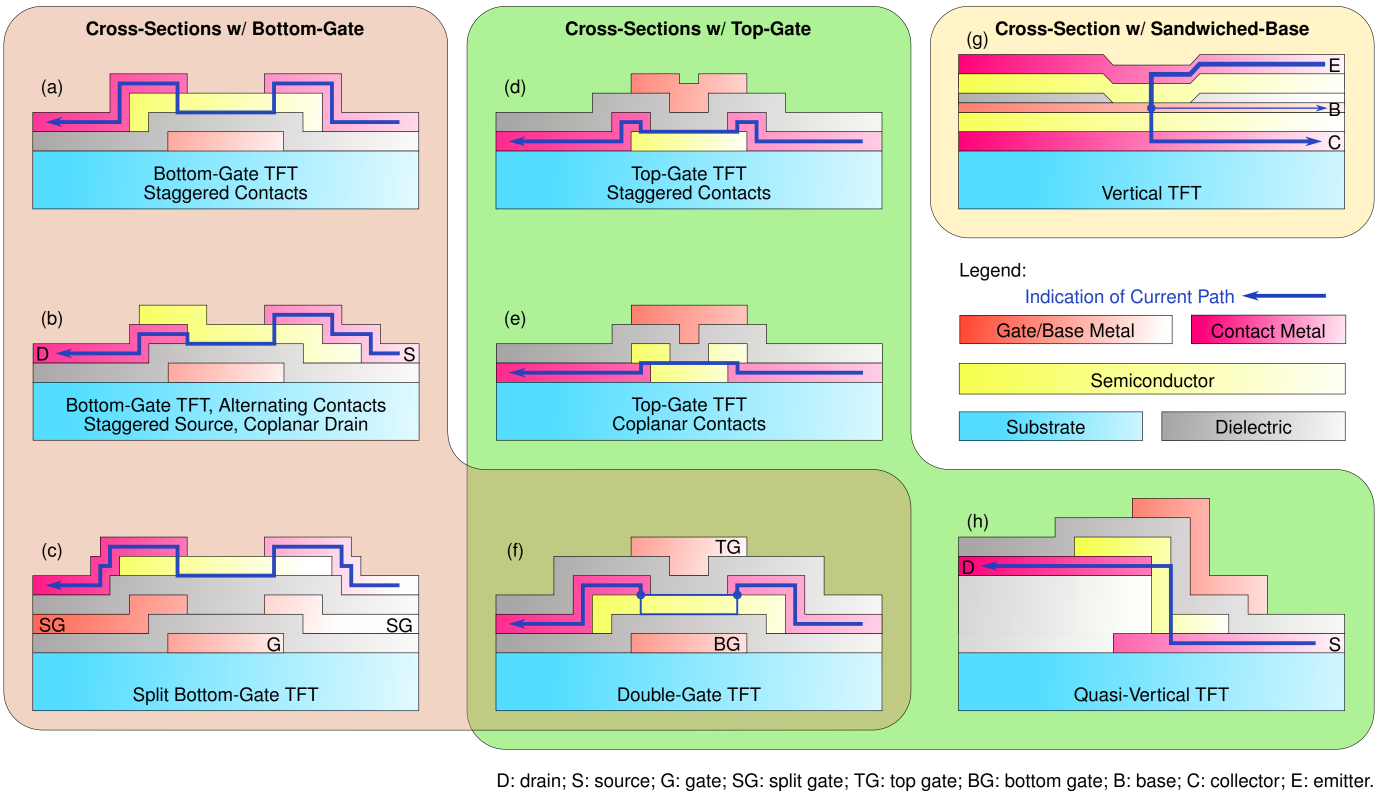

Fig. 4. TFT cross-sections. (a) Bottom-gate TFT with staggered source and drain contacts, (b) bottom-gate TFT with alternating contacts (ACTFT) [35], (c) bottom-gate TFT with a split gate [36], (d) top-gate TFT with staggered source and drain contacts [37], (e) top-gate TFT with coplanar contacts, (f) double-gate TFT with top- and bottom-gate electrodes [38], (g) vertical TFT with a current flow that is perpendicular to the layers of the transistor [39], and (h) quasi-vertical TFT [40], [41].

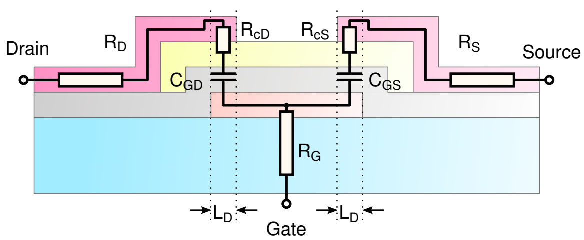

Fig. 5. Dominant parasitics of TFTs that can be optimized by the transistor layout or cross-section. Here, C_{GS} and C_{GD} are the gate-source and gate-drain capacitances, R_{cS} and R_{cD} are the contact interface resistances, R_S and R_D are the contact metal resistances, and R_G is the gate metal resistance.

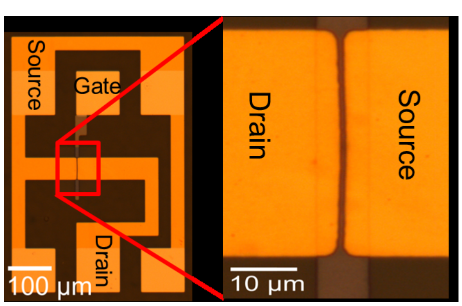

Fig. 6. A top view of a bottom-gate IGZO TFT device on a polyimide substrate with staggered contacts, a 1 µm long channel, and an f_t of 47 MHz. [5] © 2013 IEEE. Reproduced, with permission, from [5].

[54]. These technologies are fast enough for active wireless communication in RFID- or NFC-tags. Silicon thin-film transistors with mobilities exceeding those of MO-TFTs have been reported [59], [62], [64]. They also are viable for use in active RFID- and NFC-tags. However, high-performance silicon thin-film transistors tend to have a longer channel than MO-TFTs, by a factor of about 50. The longer channel is usually required to form the necessary crystalline structure in the silicon layer, limiting scalability of these technologies.

Equation (5) shows that the performance of a TFT in terms of μ_{eff} is better when the channel is longer. In contrast, the performance in terms of transconductance g_m and thus f_t (see Eq. (6)) of the TFT is better when the channel is shorter. Since a high f_t is a prerequisite for fast circuit operation, the scalability of the channel length is an important prerequisite for future improvements.

III. Metal-Oxide RF Circuits

As discussed in the preceding and summarized in Tables II and III, metal-oxide circuits provide a good compromise among speed, availability, and cost for many applications, including wireless communication systems. The competing technologies suffer from high cost in the case of thinned silicon, low performance in the case of organic and a-Si TFTs, non-uniformity across a large area and limited scalability in the case of LTPS, and lack of maturity in the case of carbon based TFTs. As a result, the research and development of metal-

IEEE MICROWAVE MAGAZINE – Vol. 23(4) – pp. 24-44

TABLE II
TRANSISTOR DEVICE PERFORMANCE REPORTED IN THE LITERATURE.

Category	**Semiconductor**	**Type**	**Ref.**	**Year**	L **in µm**	f_t **in MHz**	μ_{eff} **in** $\frac{\text{cm}^2}{\text{V·s}}$
Organic TFT	DNTT	p-type	[43]	2018	0.60	6.7	2.00
	C_8–DNBDT–NW	p-type	[44]	2018	3.00	20.0	2.10
	C_{60}	n-type	[13]	2018	0.20	40.0	0.06
	P(NDI$_2$OD–T$_2$)	n-type	[45]	2016	1.75	20.0	0.82
	C_{10}-DNTT	p-type	[36]	2014	2.00	20.0	0.40
			[46]	2014	2.00	19.0	2.50
	Rubrene	p-type	[9]	2013	4.50	25.0	5.00
	C_{60}	n-type	[12]	2011	2.00	27.7	2.22
	Pentacene	p-type	[12]	2011	2.00	11.4	0.73
Metal Oxide TFT	IGZO	n-type	[42]	2020	0.16	6.0	4.00
			[40]	2019	0.20	20.0	6.57
			[47]	2019	20.00		47.90
			[35]	2018	0.60	49.2	
			[48]	2018	0.28	80.0	1.10
			[49]	2018	100.00		20.90
			[50]	2017	20.00		9.17
			[16]	2017	10.00		76.80
			[51]	2017	5.00		20.60
			[52]	2015	20.00		12.70
			[41]	2015	0.30	1.5	0.20
			[38]	2014	7.50	5.6	9.50
			[53]	2014	5.00		11.97
			[54]	2013	0.50	135.0	7.50
			[5]	2013	1.00	47.0	
			[55]	2012	2.50	10.7	14.40
	ITO	n-type	[17]	2019	0.16	2100.0	26.00
	IZO	n-type	[56]	2020	1.50	23.0	1.40
	ZO	n-type	[57]	2019	2.00		13.00
	TZO	n-type	[58]	2016	50.00		66.70

DNTT: dinaphtho[2,3-b:2',3'-f]thieno[3,2-b]thiophene; C8-DNBDT-NW: 3,11-dioctyldinaphtho[2,3-d:2',3'-d']benzo[1,2-b:4,5-b']dithiophene; C60: Buckminsterfullerene; P(NDI2OD-T2): poly[N,N'-bis(2-octyldodecyl)-naphthalene-1,4,5,8-bis(dicarboximide)-2,6-diyl]-alt-5,5'-(2,2'-bithiophene); C10-DNTT: 2,9-di-decyldinaphtho[2,3-b:2',3'-f]thieno[3,2-b]thiophene.

oxide TFT circuits has received a great deal of attention in recent years [71]–[79].

A. TFT Modelling and Computer Aided Design

TFTs are mainly modeled in two different ways for two different purposes. First, the device geometry and materials are modeled with physical models to predict device behavior and characteristics. Second, device behavior is modeled for circuit simulation. The models for circuit simulation have to be much faster and again are either physics-based or behavioral models. Dedicated physics-based, scalable models have been developed and are widely available for silicon TFTs [80] as well as for organic TFTs [81]–[83]. This, however, is not the case for metal-oxide TFTs and carbon-based transistors. Dedicated models are still being developed for those transistor types [84]. Meanwhile, metal-oxide TFTs are frequently modeled for circuit simulation by fitting SPICE MOS-FET Level 3 [85] or models for amorphous silicon TFTs [86], such as the HSPICE Level 61 RPI a-Si TFT Model, to measured device characteristics. Simultaneously, new tools and design flows that are optimized for the special requirements of flexible circuits are being developed [87].

B. Amplifiers

Wireless communication requires fast amplifiers. The transmitting side demands a power amplifier that is matched to an antenna to broadcast a radio signal into the air. This amplifier has to operate at the carrier frequency of the wireless transmission. A very important frequency for this purpose is $f_c = 13.56\,\text{MHz}$, because it is a free ISM-band used by standardized RFID- and NFC-tags. The receiving side

TABLE III
TRANSISTOR DEVICE PERFORMANCE REPORTED IN THE LITERATURE.

Category	Semiconductor	Type	Ref.	Year	L in µm	μ_{eff} in $\frac{\mathrm{cm}^2}{\mathrm{V \cdot s}}$
Metal Oxide TFT +	IGZO	n-type	[59]	2019	6.00	13.52
+ Si TFT	LTPS	p-type	[59]	2019	6.00	81.76
Metal Oxide TFT +	IGZO	n-type	[60]	2011	10.00	16.30
+ Si TFT	LTPS	p-type	[60]	2011	10.00	69.00
Metal Oxide TFT +	IGZO	n-type	[61]	2017	3.60	10.10
+ Si TFT	LTPS	p-type	[61]	2017	100.00	78.30
Si TFT	LTPS	n-type	[62]	2005		200.00
		p-type	[62]	2005		100.00
	nc-Si:H	n-type	[63]	2009	8.00	6.42
			[64]	2006	50.00	450.00
		p-type	[64]	2006	50.00	100.00
		n-type	[28]	2005	45.00	30.00
	a-Si:H	n-type	[27]	2017	100.00	1.10
	a-Si	n-type	[65]	2010	5.00	0.33
			[66]	2007	60.00	0.25
Carbon TFT	CNT	p-type	[67]	2019	50.00	80.00
			[68]	2019	2.00	23.40
			[69]	2018	2.00	52.60
		n-type	[69]	2018	2.00	50.00
		ambipolar	[70]	2015	5.00	15.00
		p-type	[23]	2005	7.00	150.00
	Graphene	ambipolar	[22]	2012	10.00	116.00

needs a low-noise amplifier (LNA) matched to an antenna to pick up and amplify signals. The range of a wireless system is directly connected to the power the transmitting power amplifier outputs and the sensitivity/gain of the receiving LNA.

Important performance characteristics of an amplifier are the voltage gain A_V, the -3 dB-bandwidth BW, and the gain-bandwidth product GBW.

$$A_V = \frac{v_{\mathrm{out}}}{v_{\mathrm{in}}}, \tag{7}$$

where v_{in} is the input signal amplitude and v_{out} is the output signal amplitude. Toward high frequencies, the gain of amplifiers drops. The -3 dB-bandwidth BW of an amplifier is the frequency where the gain A_V has dropped by 3 dB compared to the gain in the flat band. The gain-bandwidth product GBW is defined as

$$\mathrm{GBW} = A_V \cdot \mathrm{BW}. \tag{8}$$

It tends to be constant for changing values of A_V if the technology and amplifier topology remain the same, assuming that the amplifier is well designed, meaning that an amplifier with a larger gain A_V has an accordingly smaller bandwidth BW. Consequently, the GBW is a good figure of merit to compare technologies, when the topology of the amplifiers is the same or similar.

Figure 7 presents the basic high-speed amplifier topologies that can be realized in metal-oxide TFT technologies with up to three transistors. These are the most suited for the first input stage of wireless receivers. The common-source amplifier in Fig. 7 (a) is simple yet effective, and it requires the smallest supply voltage. The cascode amplifier in Fig. 7 (b) achieves a higher gain-bandwidth product than the common-source amplifier and is tunable by adjusting the DC voltage $\mathrm{V_{casc}}$. It, however, requires roughly twice the supply voltage and consumes more power. The Cherry-Hooper amplifier in Fig. 7 (c) uses positive feedback via TFT $\mathrm{T_6}$ to achieved the highest gain-bandwidth product. It consumes the most power and requires careful design and optimization. A complementary inverter is not among the basic amplifier topologies, because metal-oxide technologies provide only n-type TFTs.

Figure 8 depicts two basic high-gain amplifier topologies with three active transistors. They provide a high gain at a lower gain-bandwidth product, compared to the topologies in Fig. 7. They are, for example, suited for sensor readout circuitry and simple processing tasks.

The differential pair amplifier in Fig. 8 (a) has a high differential gain and can be tuned by adjusting the voltage $\mathrm{V_{tail}}$ that controls the tail current source $\mathrm{T_1}$. TFTs $\mathrm{T_4}$ and $\mathrm{T_5}$ are used instead of load resistors and are in a diode-connected configuration. Differential pair amplifiers are frequently employed as input stage for operational amplifiers and for sensor readout circuitry.

The pseudo-CMOS (pCMOS) inverter in Fig. 8 (b) has a

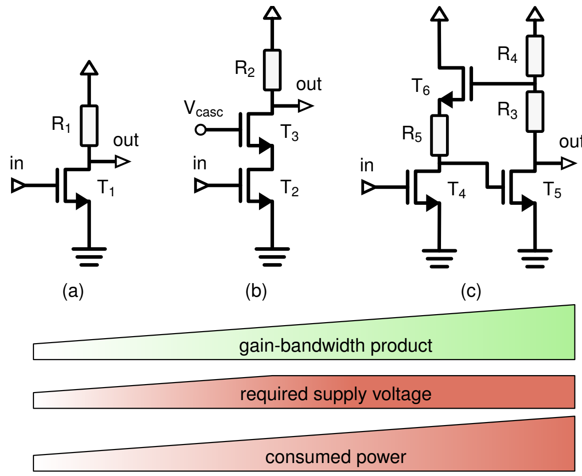

Fig. 7. Basic RF voltage amplifier circuits with only resistors and n-type TFTs: (a) Common-source amplifier, (b) cascode amplifier, and (c) Cherry-Hooper amplifier with positive feedback [88].

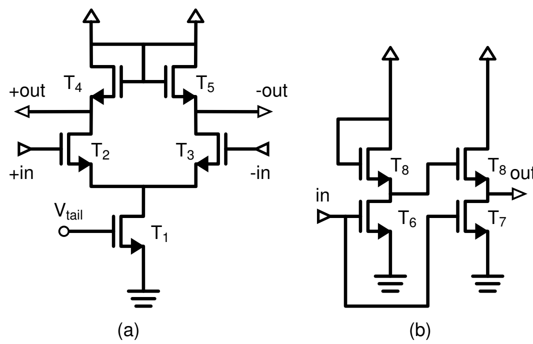

Fig. 8. Basic high-gain voltage amplifier circuits with only n-type TFTs: (a) Differential pair and (b) pseudo-CMOS amplifier [89]. Transistors T_4, T_5, and T_6 are used as an active load in the diode-connected configuration.

high gain and large output swing and is suited for digital logic circuits. It is often used for simple processing tasks. However, it consumes more power and has slower switching speeds when compared to the common-source amplifier in Fig. 7 (a), which can also be used as digital inverter.

As Fig. 8 shows, the load resistors (refer to R_1, R_2, R_3, and R_4 in Fig. 7) in amplifier circuits can be replaced by active loads (T_4, T_5, and T_6), i.e., diode-connected TFTs. This method is prominent in MO-TFT technologies, because many do not feature a high-resistance layer for the area-efficient implementation of passive resistors. The technique comes at the cost of a degraded linearity of the amplifiers [90], [91].

The ability to integrate large resistances is necessary for low power consumption as well as for bias networks of amplifiers and circuits in general. Figure 9 details biasing schemes that are used in flexible MO-technologies, which do not feature a high-resistance layer. Figure 9 (a) shows diode-connected TFT T_1, with a long channel length to achieve a high impedance in the bias network. The impedance, however, is asymmetric for the positive and negative half-waves of the signal. The DC bias itself is defined by R_1, R_2, and the supply voltage. Stacks of long-channel diode-connected TFTs appear in Fig. 9 (b). The DC bias is defined by the dimensions of T_2, T_3, T_4, and the

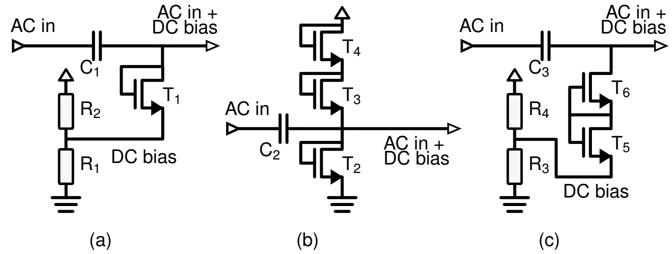

Fig. 9. Biasing schemes to overcome the lack of a high-resistance layer. (a) Diode-connected TFT, (b) stacks of diode-connected TFTs, and (c) oppositely stacked diode-connected TFTs [90].

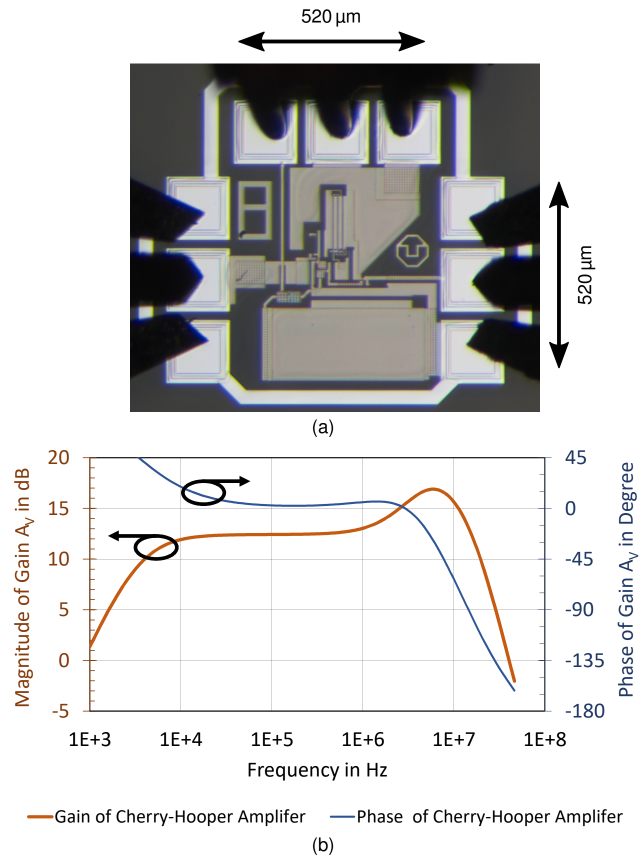

Fig. 10. (a) Contacted die and (b) frequency response of a flexible Cherry-Hooper amplifier. About one third of the core area is used by one capacitor (the area at the bottom), which is part of the biasing scheme (compare [92]).

supply voltage. Figure 9 (c) illustrates the use of oppositely stacked diode-connected TFTs [90] as high impedance in the bias network. The latter scheme does not need to use long channel devices. Instead, it exploits the drain current leakage of transistors T_5 and T_6. It can be used to integrate extremely high impedances and can be employed only in technologies that have appropriately "large" drain currents at $V_{\rm GS} = 0$, which would usually be considered an unwanted parasitic.

Figure 10 shows the die and frequency response of a Cherry-Hooper amplifier [92]. It has a gain-bandwidth product of about 50 MHz, which means it has a voltage gain of 11 dB in the important 13.56 MHz ISM band. Table IV summarizes the performance of flexible MO-TFT amplifiers reported in the literature.

TABLE IV
A SELECTION OF REPORTED GAIN BANDWIDTH PRODUCTS (GBWS) OF FLEXIBLE AMPLIFIERS.

Category	**Semiconductor**	**Ref.**	**Year**	**Topology**	V_{DD} **in V**	**GBW in MHz**	**Gain in dB**
Metal Oxide TFT	IGZO	[92]	2020	Cherry-Hooper	8	49.35	19.38
		[92]	2020	4-Stage Common-Source	8	33.43	28.90
		[93]	2019	Operational Amplifier	15	0.28	29.54
		[94]	2019	Operational Amplifier	±10	7.50	23.52
		[95]	2018	Operational Amplifier	10	0.20	10.00
		[96]	2018	Operational Amplifier	13	0.09	24.90
		[97]	2018	Operational Amplifier	10	0.04	22.00
		[86]	2017	Cherry-Hooper	6	7.16	9.50
		[98]	2017	Operational Amplifier	±10	0.01	14.00
		[99]	2015	Operational Amplifier	±15	0.10	24.50
		[100]	2015	Operational Amplifier	6	0.22	19.00
		[101]	2014	Common-Source	6	0.56	17.00
		[101]	2014	Cascode	6	3.91	25.00
		[102]	2014	Cherry-Hooper	6	11.59	10.40
		[102]	2014	2-Stage Cherry-Hooper	6	18.50	33.30
		[103]	2014	Operational Amplifier	5	0.08	22.50
		[104]	2013	Operational Amplifier	5	0.93	18.70
		[85]	2013	2-Stage Cascode	6	9.17	10.00
		[85]	2013	3-Stage Common-Source	6	2.37	10.00
		[55]	2012	Cascode	5	2.06	7.80
		[55]	2012	Common-Source	5	2.63	6.80
Hybrid Complementary	IGZO + LTPS	[20]	2019	Operational Amplifier	±20	68.55	50.70
Metal Oxide TFT + Si TFT		[59]	2019	CMOS Inverter	8	11.40	
Si TFT	a-Si:H	[25]	2010	Operational Amplifier	25	0.27	42.50

C. Oscillators

Oscillator circuits are required for wireless communication to synthesize carrier, baseband, and modulation frequencies. Ring oscillators, in particular, are a widely used and convenient circuits to verify the performance of a technology. Their design is relatively simple, their output frequency f_{osc} is easy to characterize, and their stage delay τ can be directly calculated from the observed frequency of oscillation:

$$\tau = \frac{f_{\mathrm{osc}}}{2 \cdot n}, \tag{9}$$

where n is the number of stages.

The ring oscillator topology can be easily implemented in many technologies and permits the comparison of flexible technologies. Many parasitic layout effects are automatically included in these comparisons. For example, a technology that lacks low-ohmic low-capacitive interconnect layers will not be able to produce a fast ring oscillator, even if the transistors promise excellent performance by having a high f_t. Thus, the gate delay τ of ring oscillators has become a common performance benchmark in the flexible domain and others [83]. Table V reviews flexible ring oscillator gate delays reported in the literature.

Ring oscillators must have an odd number n of inverting stages. The shortest possible ring oscillator has three stages. From Table V and Eq. (9), it follows that the fastest MO-TFT three-stage ring oscillator using the reported technologies [105] oscillates at 15.19 MHz and barely covers the free ISM band at 13.56 MHz. However, in a real system, a ring oscillator with five or more stages is preferable, because ring oscillators with more stages operate more reliably.

IV. WIRELESS APPLICATIONS IN FLEXIBLE TECHNOLOGIES

In the past decade, flexible technologies have made great advances. Their speed and reliability have reached a point where wireless applications begin to become realistic. At the same time, the achievable complexities and variety of compatible flexible components, such as sensors, actuators, batteries, and solar cells have greatly increased. The Internet of Things (IoT), RFID-tags, and NFC-tags will influence many future applications. Wireless transceivers will be required to enable data transmissions at all times. Flexibility will be the enabler for seamless integration into our daily lives.

The most challenging technical component for flexible wireless systems is the transmitter (Tx). It has to provide power gain at radio frequencies. To be able to communicate

IEEE MICROWAVE MAGAZINE – Vol. 23(4) – pp. 24-44

TABLE V
REPORTED RING OSCILLATOR AND INVERTER PERFORMANCE.

Categroy	**Semiconductor**	**Reference**	**Year**	V_{DD} **in V**	τ **in ns**	$1/2\tau = f_{osc}/n$ **in MHz**
Metal Oxide TFT	IGZO	[106]	2019	5	230	2.17
		[16]	2017	20	108	4.63
		[107]	2017	4	48	10.32
		[51]	2017	20	21	23.56
		[50]	2017	10	1370	0.36
		[108]	2016	20	106	4.73
		[109]	2016	10	29	17.29
		[110]	2015	6	3199	0.16
		[105]	2015	20	11	45.57
		[111]	2014	20	58	8.59
		[112]	2013	6	17361	0.03
		[113]	2011	20	479	1.04
		[114]	2011	22	17	29.41
		[115]	2010	25	48	10.50
	IZO	[116]	2017	5	344	1.45
Hybrid Complementary MO-TFT + Organic TFT	IGZO + C_{60}	[117]	2008	10	500000	0.001
Si TFT	a-Si:H	[118]	2009	6	3333	0.15
Organic TFT	DNTT	[43]	2018	3	79	6.33
	DNTT + PDI8CN2	[119]	2015	12	66667	0.01
	CP-DIPS:PTAA	[120]	2015	20	71429	0.01
Carbon TFT	CNT	[68]	2019	3	23	21.74
		[69]	2018	6	6	87.72

PDI8CN2: N,N'-bis(n-octyl)-dicyanoperylene-3,4:9,10-bis(dicarboximide);
CP-DIPS:PTAA: blend of 6,13-bis[(cyclopropyldiisopropylsilyl)ethynyl] pentacene and poly(triarylamine).

with standard devices, such as RFID, NFC, and IoT devices, the requirement is $f_c \geq 13.56\,\mathrm{MHz}$. Close proximity links are also frequently operated at $f_c = 125\,\mathrm{kHz}$.

The second most challenging and final technical component for flexible wireless systems is the receiver (Rx). It must have a high sensitivity to wireless signals at the previously mentioned carrier frequencies. The receiver is simpler than the transmitter, because it does not have to provide a high gain at the carrier frequency as long as it does not add noise and efficiently demodulates the baseband signal [90]. Afterward, the baseband signal, which is at a much lower frequency, can be easily amplified. However, for the highest sensitivities and thus communication ranges, high-speed transistors with gain at the carrier frequency are needed.

Flexible wireless receivers have been demonstrated in different technologies. For example, a quadrature amplitude modulation (QAM) receiver front end for 2.45 GHz ISM band and a 5 GHz six-port receiver front end based on flexible graphene diodes was shown [121], [122]. On a flexible thinned silicon substrate, a power amplifier with 10 dB gain at 5.5 GHz was introduced [121], [123] (see Fig. 11). In metal-oxide technologies amplitude modulation (AM) receivers up to a carrier frequency of 20 MHz have been demonstrated [6], [90], [124]. Several RFID and NFC tags and transponder chips have been demonstrated in flexible organic technologies [78], [125]–[128] as well as in flexible metal-oxide technologies [33], [109], [129]–[135]. Some of these solutions are powered by a 13.56 MHz conventional base station proximity field. However, they are all similar to passive, chipless remote sensing solutions [136] in the sense that they do not have an active circuit block operating at the carrier frequency, given the limited performance of the technologies that are used. Typically the only flexible component that sees the full carrier frequency is the rectifier, which harvests the energy required to power up the tag or transponder.

Two of the reported metal-oxide chips for wireless tags stand out [109], [129], because they are compatible with the data rates required by the ISO NFC standards. They are able to handle standardized baseband communication in wireless tags. Figure 12 shows such an NFC transponder chip. The work in [129] is also of interest since it features a frequency divider that directly takes the 13.56 MHz carrier frequency as input and divides it down to the 847.5 kHz required for the tag's internal clock. As a consequence, the tag clock is synchronized with the reader clock, which enables ISO-compliant data transfer.

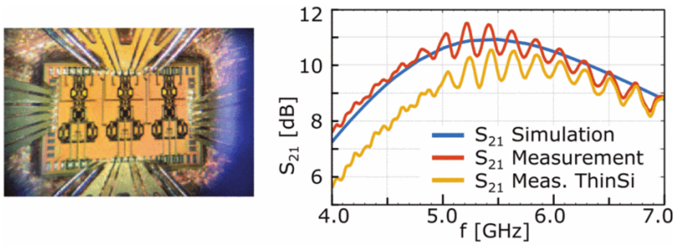

(a) (b)

Fig. 11. Silicon BiCMOS amplifier for 5 – 6 GHz thinned to 45 µm. (a) Die photo. (b) Simulated (blue), measured not-thinned (orange) and measured thinned (yellow) forward gain. [121], [123] © 2017 IEEE. Reproduced, with permission, from [121].

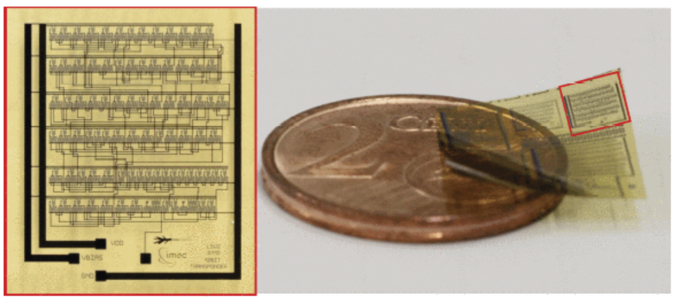

(a) (b)

Fig. 12. (a) Flexible thin-film NFC transponder chip exhibiting data rates compatible with ISO NFC standards, using self-aligned metal-oxide TFTs. It has a footprint of 3.42 mm × 3.19 mm. (b) Substrate carrying the NFC transponder chip at the top right (marked with a red border). [109] © 2016 IEEE. Reproduced, with permission, from [109].

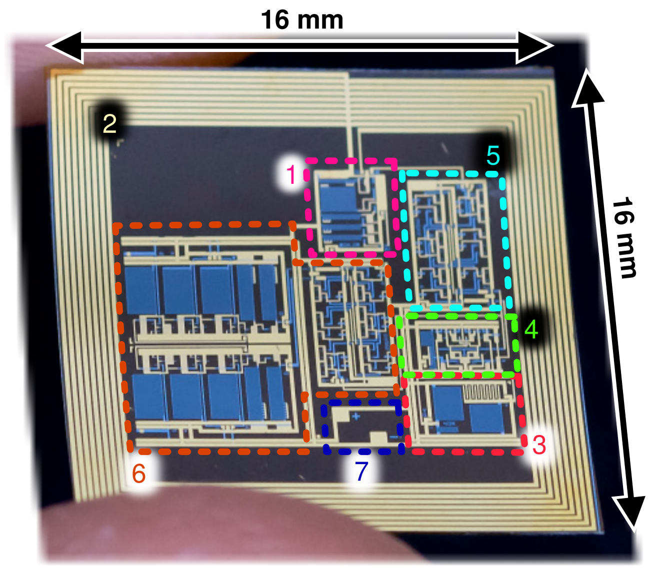

Fig. 13. Prototype of a fully flexible, fully integrated moisture sensor with an OOK transmitter on a 50 µm polyimide substrate. It has an area of 16 × 16 mm^2 and includes (1) an OOK-modulator with a DCO, (2) an antenna, (3) a moisture sensor, (4) a clocked comparator, (5) a latch, (6) a low-frequency oscillator, and (7) supply voltage pads.

V. FLEXIBLE WIRELESS MOISTURE SENSOR

In this section, as an example of the next generation of flexible wireless electronics, an active flexible wireless moisture sensor and details about its blocks illustrate how flexible metal-oxide electronics can be used to realize an active wireless sensor tag. This wireless sensor system was designed and characterized by the authors. It distinguishes itself from previous works, because it actively transmits sensor data via a carrier frequency that is generated on-chip by the flexible sensor itself.

A. System and Technology Overview

The device shown Figs. 1 and 13 is a fully integrated moisture sensor with a wireless on-off-keying (OOK) transmitter and an antenna. Many solutions to read out such sensors would use proximity links of a few centimeters, such as RFID and NFC, to read out data. In those cases, communication is managed and driven by a base station or data reader. The presented system, however, has the potential for a stand-alone flexible wireless communication system with a matched flexible receiver [90], [124]. Thanks to the active nature of the wireless moisture sensor, it can achieve a larger range than RFID- and NFC-based solutions. With expected improvements of flexible TFT performance, the carrier frequency for the data transmission of such sensors will increase, which will expand the devices' communication range, reduce antenna sizes, and thus advance the equipment's feasibility and attractiveness for real-world applications.

The wireless moisture sensor was fabricated in a flexible IGZO TFT technology [1], [55] on a 50 µm polyimide substrate. The semiconducting IGZO layer is deposited at room temperature and its mobility exceeds 10 $cm^2/(V{\cdot}s)$. It features two interconnect layers [1] with moderate parasitics. It does not have a high-resistance layer. Instead, the chromium bottom-gate metallization is used to implement resistors. The resistors are visible in Fig. 1 as gray areas. It can be seen that, because of the lack of a high-resistance layer, the resistors cover as much as half the active area. Circuit simulations and optimizations have been done using a fitted amorphous silicon TFT model [86].

The circuit consists of the moisture sensor, sensor readout circuitry, and a wireless transmitter. The sensor readout is performed by a pseudo-CMOS clocked comparator, latch, and low frequency oscillator. The low frequency oscillator provides a 50 kHz signal, which is used for two purposes. It generates the baseband frequency and duty cycles the sensor read out circuitry to save power. An even slower oscillator [137] could be used to further reduce the power consumption. This would however affect system latency. The wireless transmitter consists of a digitally controlled oscillator (DCO), the OOK modulator, and an antenna.

The DCO is used to generate the carrier frequency, and it has an average frequency of oscillation of 1.36 MHz and a digitally controllable tuning range of 15 %. This tunability can be exploited to compensate for manufacturing variations, and it can be used to realize an application with several channels. The OOK modulator successfully modulates a 200 mV_{pp} carrier with the 50 kHz baseband signal and a modulation index of around 50 %. The clocked comparator achieves 28 dB open-

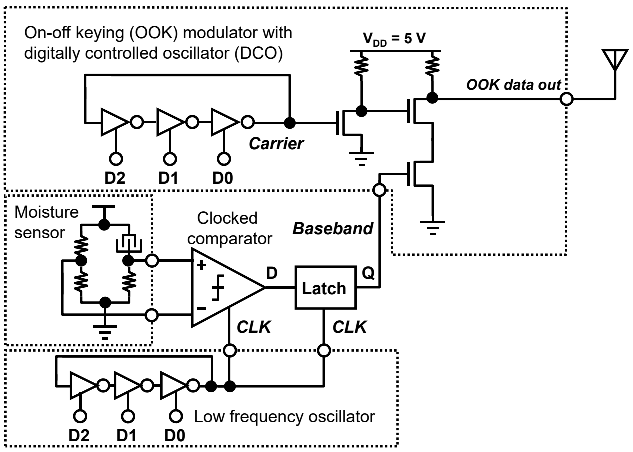

Fig. 14. System level of the wireless moisture sensor.

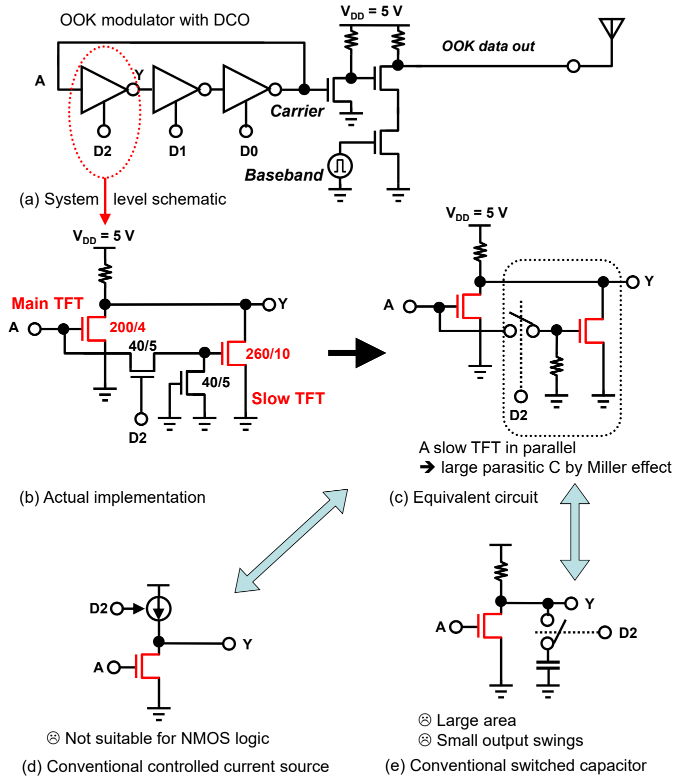

Fig. 15. On-off keying modulator with a digitally controlled ring oscillator. (a) System level, (b) transistor-level implementation of the tunable inverter stage, (c) simplified equivalent circuit of the tunable inverter stage, (d) incompatible conventional implementation with a controlled current source, and (e) incompatible conventional implementation using a switched capacitor.

loop gain with a minimum input offset of 25 mV. To characterize the moisture sensor, a small drop of tap water is placed on the device's interdigitated electrodes. The water drop, covering the sensor area of 0.44 mm^2 raises the differential output voltage from 0.28 mV to 1.60 V, which can easily be detected by the comparator.

The system was specified for and characterized with a 5 V supply. This supply voltage can be provided, for example, by flexible printed batteries (refer to Figs. 3 (b) and 3 (c)), flexible organic solar cells, and energy harvesting modules, such as the solar power module in Fig. 3 (g).

The functional blocks of the wireless moisture sensor are highlighted in Fig. 13. They are also shown on a simplified system level in Fig. 14.

B. OOK Modulator With DCO Utilizing the Miller Effect

As shown in Fig. 15 (c), an uncommon approach has to be taken to realize a digitally-controlled delay line with only an n-type thin-film transistor. Each inverter stage consists of a main TFT (L=4 µm), a slow TFT (L=10 µm), and two more TFTs (L=5 µm). The slow TFT has a large parasitic capacitance due to the Miller effect and provides sufficient gain to the inverter stage. Conventional implementations of digitally controlled ring oscillators have used controlled current sources or switched capacitors Figs. 15 (d) and 15 (e), which are not suitable for MO-TFT technologies, because these solutions are not compatible with n-type-only logic or require a very large area, while achieving only small output swings.

Figure 16 depicts the circuit and its transistor-level schematic, including the measurement configuration. The carrier signal is modulated by the 50 kHz baseband signal and has a 300 mV output swing (V_{On}) during the baseband on-state. The output swing (V_{Off}) drops below 100 mV in the baseband off-state. The baseband waveform and OOK-modulated waveform appear in Fig. 17 (a). The measured waveform includes a largeswing baseband frequency component, which is filtered by the antenna. By adjusting inputs D_0, D_1, and D_2, the oscillation frequency and thus the carrier frequency can be tuned in a range of 15 % around the center frequency of 1.36 MHz. The oscillation frequency tuning with the inputs is shown in Fig. 17 (b). The figure shows that the originally simulated tuning range of 29 % was wider than the actually achieved one.

C. Pseudo-CMOS Clocked Comparator

Figure 18 (a) shows the fabricated pseudo-CMOS comparator block. The transistor-level schematic of the clocked comparator is given in Fig. 18 (b). It employs the high-gain pseudo-CMOS structure, which enables a cross-coupled topology that obtains a high open-loop gain. The reset switches M3' and M4' driven by the clock CLK connect the outputs of the differential amplifier to the "Tail" node. This realizes a stable reset function with only n-type TFTs. A dummy load is used on the left output to improve the matching and thus the offset voltage of the comparator. The measurement configuration and results are in Fig. 19, confirming that the clocked comparator operates correctly with an input swing of only $\pm$100 mV. Fig. 19 (c) describes the frequency response and offset voltage of the clocked pseudo-CMOS comparator. The open-loop gain reaches 28 dB, with an input offset voltage of $\leq$ 75 mV.

The clock signal CLK is generated by a low-frequency oscillator. Implementing the synthesis of a low frequency is challenging in this technology. A typical analog solution requires a large chip area. A digital implementation based on a counter consumes a considerable amount of power and chip

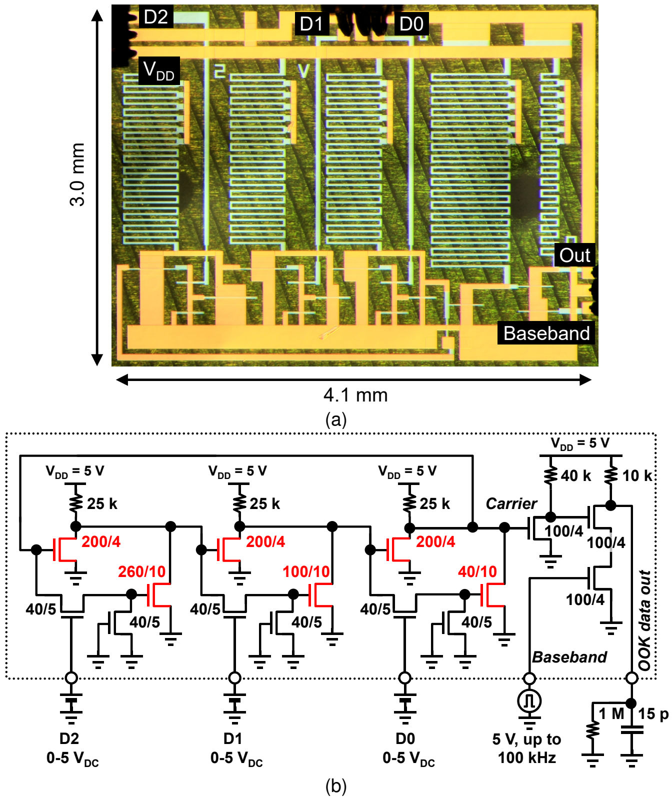

Fig. 16. On-off keying modulator with a digitally controlled ring oscillator. (a) Die and (b) transistor-level schematic, including the measurement configuration.

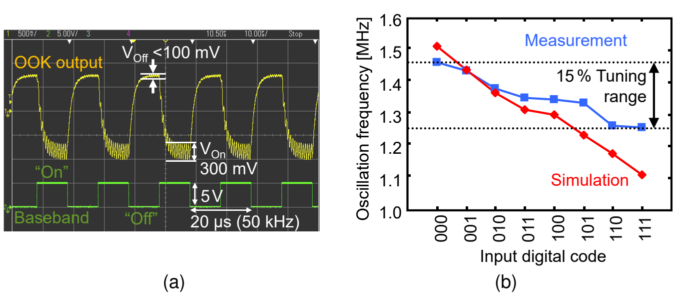

Fig. 17. Digitally controlled ring oscillator measurements. (a) Output OOK waveform and (b) tuning range of the oscillation frequency.

area. Therefore, the clock synthesis is realized by two digitally controlled ring oscillators with relatively high frequencies of oscillation f_1 and f_2. A latch is then used to pick up the much lower beat frequency $f_{\text{beat}} = f_{\text{CLK}} = f_1 - f_2 \approx 50\,\text{kHz}$, which is the interference of the outputs of the two tunable ring oscillators.

D. Moisture Sensor

The moisture sensor appears in Fig. 20. It consists of a bridge structure with interdigitated electrodes detecting open/short in the top metal layer and three resistors. When the electrodes are open without moisture, the output node is pulled down. The reference "Ref" is set to roughly 0.5 V, which is the result of co-optimization with the clocked comparator. The sensor is characterized by using a small drop of tap water.

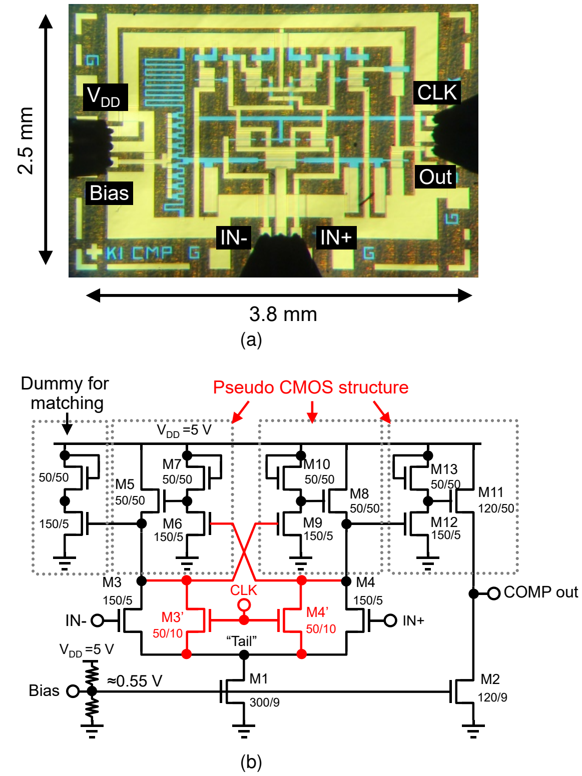

Fig. 18. Clocked pseudo-CMOS comparator. (a) Die and (b) transistor-level schematic.

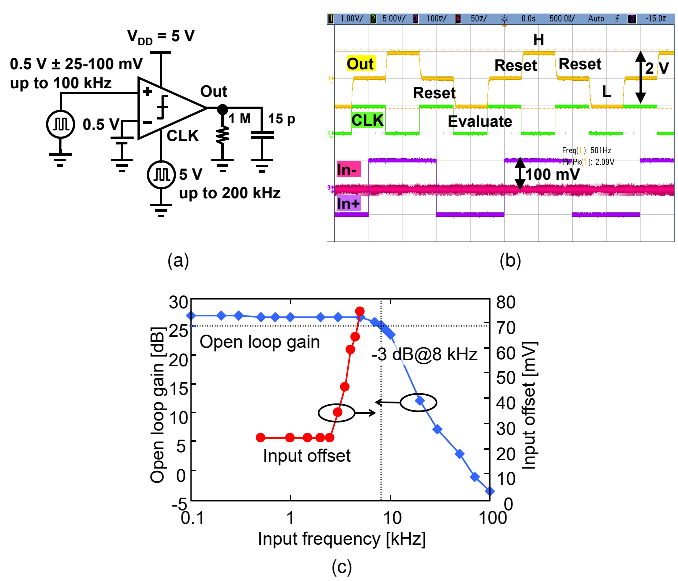

Fig. 19. Operation of the clocked pseudo-CMOS comparator. (a) Measurement configuration, (b) measured waveforms, and (c) frequency response and input offset voltage.

The water drop, covering the sensor area of 0.44 mm^2 (see Figs. 20 (c) and 20 (d)), raises the output from 0.28 mV to 1.60 V, which is then picked up by the comparator as shown in Fig. 14.

TABLE VI
COMPARISON OF PRESENTED FLEXIBLE WIRELESS MOISTURE SENSOR TO FLEXIBLE WIRELESS TAGS REPORTED IN THE LITERATURE.

Process Category	TFT Type(s)	Ref.	Year	Application	V_{DD}	Carrier Frequency	BW / Data rate	Coupling	Remarks
Metal Ox.	n-type	**This work**	2021	Sensor w/ OOK Tx	5 V	1.36 MHz 15 % tuning	≈ 50 kb/s	Inductive / Radio wave	**Built-in oscillator for carrier frequency synthesis**
Metal Ox.	n-type	[130]	2018	CAPID tag	0.3 V	2.00 MHz (external)	890 b/s	Capacitive	
Metal Ox.	n-type	[131]	2018	CAPID tag	≈ 2.5 V	1.00 MHz (external)	5.8 kb/s	Capacitive	
Metal Ox.	n-type	[135]	2017	RFID tag	20 V	13.56 MHz (external)	13.19 kb/s	Inductive	148 kb/s @ 2 V pseudo-CMOS
Metal Ox.	n-type	[129]	2017	RFID / NFC tag	3 V	13.56 MHz (external)	105.9 kb/s	Inductive	Vbias = 6 V, CLK=847.5 kHz, direct clock division of 13.56 MHz carrier, ISO14443-A compliant
Metal Ox.	n-type	[33] [132]	2015	RFID / NFC tag	2 V	13.56 MHz (external)	71.6 kb/s	Inductive	ISO15693 compatible datarates
Organic Organic	p-type n-type	[127]	2015	RFID tag	24 V	13.56 MHz (external)	50 b/s	Inductive	With envelope detector
Organic	p-type	[138]	2014	Medical sensor	2 V	13.56 MHz (external)	3 Hz	Inductive	Back scattering
Organic Metal Ox.	p-type n-type	[126]	2012	RFID tag	10 V	13.56 MHz (external)	20.6 kb/s	Inductive	Code generator can operate with 3.75 V
Organic Metal Ox.	p-type n-type	[139] [126]	2012	RFID tag	10 V	13.56 MHz (external)	20.6 kb/s	Inductive	Code generator can operate with 3.75 V
Organic	p-type	[78]	2009	RFID tag	14 V	13.56 MHz (external)	787 b/s	Inductive	
Organic	p-type	[128] [140]	2006	RFID tag	30 V	13.56 MHz (external)	1 kb/s	Capacitive	First organic RFID tag

RFID: radio-frequency identification; CAPID: capacitive RFID; NFC: near-field communication.

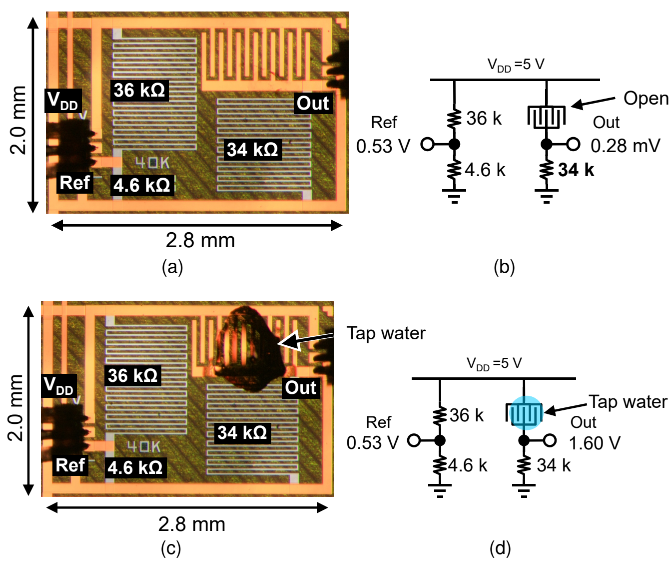

Fig. 20. Moisture sensor block. (a) Dry moisture sensor die, (b) schematic and measured output voltages of dry moisture sensor, (c) moisture sensor wet by a drop of tap water, and (d) schematic and measured output voltages of wet moisture sensor.

E. Conclusion for Wireless Moisture Sensor System

To date, such wireless sensor systems usually require external carrier signal generation, because the technologies are generally too slow to generate, for example, a 13.56 MHz carrier signal on-chip. The wireless moisture sensor discussed above is one of the first attempts to make a fully integrated active flexible wireless system in metal-oxide technology. Table VI compares the presented wireless moisture sensor to previous flexible wireless tags reported in the literature. As described in the previous section, the moisture sensor can generate a carrier signal of 1.36 MHz and would require a tenfold speed improvement to operate in the free ISM band at 13.56 MHz. It was fabricated in a technology that has an f_t of 10.7 MHz [1], [55]. As Table II shows, MO-TFT technologies with more than a tenfold improvement have been demonstrated. Implementing the presented wireless moisture sensor in one of those would enable its operation at higher frequencies, facilitating the use of free ISM bands and increasing the range of the wireless moisture sensor, today.

VI. CONCLUSION AND OUTLOOK

Different flexible electronic technologies are currently being researched and developed. Among them, the metal-oxide based TFTs provide an attractive compromise for future wireless applications, because they offer good performance, cost, scalability, uniformity, and maturity.

The performance of flexible organic technologies falls far behind that of metal-oxide technologies. Silicon thin-film technologies are promising, but they are more complex than metal-oxide technologies and do not scale well. Carbon-based TFT technologies are also promising but lack maturity. Flexible thinned silicon ICs electrically outperform the other flexible technologies, but are also the most complex and expensive.

Complex analog and digital applications can be realized on flexible substrates with up-to-date metal-oxide based thin-film technologies. However, analog circuits for wireless communication require high operation frequencies, because otherwise prohibitively large antennas are required or the communication range is lacking. The operation frequencies needed for active wireless communication are not easily achieved with the available flexible metal-oxide technologies. Operation in the megahertz regime needs further technological improvements as well as clever system and circuit design.

The authors' wireless moisture sensor, which has been presented in Section V, demonstrates the possibilities offered by flexible metal-oxide technologies. It integrates all the needed circuitry and a sensor element on a fully flexible plastic substrate. In contrast to previous works, it incorporates a ring oscillator for carrier frequency synthesis, which enables active radio transmissions. The presented results show that the employed technology is not fast enough to reach the ISM band at 13.56 MHz. Implementing the same tag in one of the fastest reported metal-oxide technologies, would provide a sufficient performance increase to enable the tag to communicate in the 13.56 MHz band, without changes to the presented system design.

The circuit blocks integrated in the presented moisture sensor tag are an on-off-keying modulator, a digitally controlled oscillator, a moisture sensor, a pseudo-CMOS clocked comparator, a latch, and a low-frequency oscillator. The integrated digitally controlled oscillator synthesizes a carrier frequency of 1.36 MHz on-chip. The on-off-keying modulator block is able to modulate this carrier with a 50 kHz baseband signal and modulation index of around 50 %. The integrated clocked comparator is triggered by the signal of the low-frequency oscillator and reads out the sensor state, thus generating the baseband signal. It has a 28 dB open-loop gain.

Numerous works on flexible oscillators have been reported in the literature. A selection of reported ring oscillators was summarized in this article. These circuits are frequently used to benchmark the high-frequency performance of flexible TFT technologies. They also act as local oscillators in communication circuits. However, realizing oscillators for megahertz frequencies is challenging in metal-oxide technologies and extraordinarily difficult in organic ones.

Ultimately, flexible circuits may never be able to compete with the speed and complexity of rigid integrated circuits. However, flexible electronics already outperform conventional electronics in terms of mechanical properties, cost, and application specific requirements in the field of wearables, biomedical applications, disposable devices, and the Internet of Things. Soon, the ability to realize reliable wireless communication in these flexible devices will enable these technologies to open up a vast number of new applications.

ACKNOWLEDGMENT

The first and second author equally contributed to this article. The authors would like to thank the German Research Foundation (DFG) for creating the FFlexCom priority program SPP 1796 – High Frequency Flexible Bendable Electronics for Wireless Communication Systems. This priority program is dedicated to supporting the research and development of flexible wireless systems across all technology groups presented in this work. Parts of this work have been supported by DFG's SPP 1796 under projects Wireless Indium-Gallium-Zink-Oxide Transceivers and Devices On Mechanically-Flexible Thin-Film Substrates II (WISDOM II) and Coordination Funds 2. The authors want to thank the Center for Tactile Internet With Human-in-the-Loop (CeTI) Excellence Cluster for inspiring discussions regarding flexible electronics and applications. The authors extend special thanks to S. Knobelspies and G. Cantarella for the fabrication of the presented wireless moisture sensor at the Swiss Federal Institute of Technology Zurich, Zurich, Switzerland. G. Cantarella is currently with the Free University of Bolzano, Bozen-Bolzano, Italy.

REFERENCES

[1] G. Cantarella, K. Ishida, L. Petti, N. Münzenrieder, T. Meister, R. Shabanpour, C. Carta, F. Ellinger, G. Tröster, and G. A. Salvatore, "Flexible in–ga–zn–o-based circuits with two and three metal layers: Simulation and fabrication study," *IEEE Electron Device Letters*, vol. 37, no. 12, pp. 1582–1585, Dec. 2016.

[2] K. Nomura, H. Ohta, A. Takagi, T. Kamiya, M. Hirano, and H. Hosono, "Room-temperature fabrication of transparent flexible thin-film transistors using amorphous oxide semiconductors," *Nature*, vol. 432, no. 7016, pp. 488–492, Nov. 2004. [Online]. Available: https://doi.org/10.1038/nature03090

[3] C. A. Neugebauer, "Tensile properties of thin, evaporated gold films," *Journal of Applied Physics*, vol. 31, no. 6, pp. 1096–1101, 1960. [Online]. Available: https://doi.org/10.1063/1.1735751

[4] Y. Umeno, A. Kushima, T. Kitamura, P. Gumbsch, and J. Li, "Ab initio study of the surface properties and ideal strength of (100) silicon thin films," *Phys. Rev. B*, vol. 72, p. 165431, Oct. 2005. [Online]. Available: https://link.aps.org/doi/10.1103/PhysRevB.72.165431

[5] C. Carta, K. Ishida, B. K. Boroujeni, R. Shabanpour, T. Meister, G. Schmidt, E. Suomalainen, A. Brandlmaier, G. A. Salvatore, N. Münzenrieder, L. Petti, G. Tröster, D. Petrantonakis, D. Kozakis, R. Paradiso, M. Krebs, M. Tuomikoski, H.-J. Egelhaaf, and F. Ellinger, "Overview of the ec project flexibility: Organic and thin-film ics up to radio frequencies for multifunctional flexible systems (invited)," in *SBMO/IEEE MTT-S International Microwave and Optoelectronics Conference (IMOC)*, Rio de Janeiro, Brazil, Aug. 2013. [Online]. Available: https://publications.meistertilo.de/wp-content/uploads/2018/08/130804_Carta_copyright_doi.pdf

[6] T. Meister, K. Ishida, C. Carta, R. Shabanpour, B. K.-Boroujeni, N. Münzenrieder, L. Petti, G. A. Salvatore, G. Schmidt, P. Ghesquiere, S. Kiefl, G. De Toma, T. Faetti, A. C. Hübler, G. Tröster, and F. Ellinger, "3.5mw 1mhz am detector and digitally-controlled tuner in a-igzo tft for wireless communications in a fully integrated flexible system for audio bag," in *2016 IEEE Symposium on VLSI Circuits (VLSI-Circuits)*, Jun. 2016, pp. 1–2.

[7] "Multi circuit boards," accessed 30.12.2020. [Online]. Available: https://www.multi-circuit-boards.eu/en/products/printed-circuit-boards/flexible-pcb.html

[8] "Flexpcb," accessed 30.12.2020. [Online]. Available: https://flexpcb.com/

[9] M. Uno, T. Uemura, Y. Kanaoka, Z. Chen, A. Facchetti, and J. Takeya, "High-speed organic single-crystal transistors gated with short-channel air gaps: Efficient hole and electron injection in organic semiconductor crystals," *Organic Electronics*, vol. 14, no. 6, pp. 1656 – 1662, 2013. [Online]. Available: http://www.sciencedirect.com/science/article/pii/S1566119913001146

[10] J. T. E. Quinn, J. Zhu, X. Li, J. Wang, and Y. Li, "Recent progress in the development of n-type organic semiconductors for organic field effect transistors," *J. Mater. Chem. C*, vol. 5, pp. 8654–8681, 2017. [Online]. Available: http://dx.doi.org/10.1039/C7TC01680H

[11] T. Okamoto, S. Kumagai, E. Fukuzaki, H. Ishii, G. Watanabe, N. Niitsu, T. Annaka, M. Yamagishi, Y. Tani, H. Sugiura, T. Watanabe, S. Watanabe, and J. Takeya, "Robust, high-performance n-type organic semiconductors," *Science Advances*, vol. 6, no. 18, 2020. [Online]. Available: https://advances.sciencemag.org/content/6/18/eaaz0632

[12] M. Kitamura and Y. Arakawa, "High current-gain cutoff frequencies above 10 MHz in n-channel c60 and p-channel pentacene thin-film transistors," *Japanese Journal of Applied Physics*, vol. 50, p. 01BC01, Jan. 2011. [Online]. Available: https://doi.org/10.1143%2Fjjap.50.01bc01

[13] B. Kheradmand-Boroujeni, M. P. Klinger, A. Fischer, H. Kleemann, K. Leo, and F. Ellinger, "A pulse-biasing small-signal measurement technique enabling 40 mhz operation of vertical organic transistors," *Scientific Reports*, vol. 8, no. 1, p. 7643, May 2018. [Online]. Available: https://doi.org/10.1038/s41598-018-26008-0

[14] B. Kheradmand-Boroujeni, G. C. Schmidt, D. Höft, K. Haase, M. Bellmann, K. Ishida, R. Shabanpour, T. Meister, C. Carta, A. C. Hübler, and F. Ellinger, "Small-signal characteristics of fully-printed high-current flexible all-polymer three-layer-dielectric transistors," *Organic Electronics*, vol. 34, pp. 267 – 275, 2016. [Online]. Available: http://www.sciencedirect.com/science/article/pii/S1566119916301835

[15] B. Kheradmand-Boroujeni, G. C. Schmidt, D. Hoft, R. Shabanpour, C. Perumal, T. Meister, K. Ishida, C. Carta, A. C. Hubler, and F. Ellinger, "Analog characteristics of fully printed flexible organic transistors fabricated with low-cost mass-printing techniques," *IEEE Transactions on Electron Devices*, vol. 61, no. 5, pp. 1423–1430, May 2014.

[16] S. Lee, J. Shin, and J. Jang, "Top interface engineering of flexible oxide thin-film transistors by splitting active layer," *Advanced Functional Materials*, vol. 27, no. 11, p. 1604921, 2017. [Online]. Available: https://onlinelibrary.wiley.com/doi/abs/10.1002/adfm.201604921

[17] M. Wang, R. Huang, Y. Wu, M. Tian, Z. Zhang, S. Li, R. Wang, C. Gu, X. Shan, X. Xiong, and X. Li, "High performance gigahertz flexible radio frequency transistors with extreme bending conditions," in *2019 IEEE International Electron Devices Meeting (IEDM)*. IEEE, Dec. 2019. [Online]. Available: https://doi.org/10.1109/iedm19573.2019.8993531

[18] N. Münzenrieder, C. Zysset, L. Petti, T. Kinkeldei, G. A. Salvatore, and G. Tröster, "Room temperature fabricated flexible nio/igzo pn diode under mechanical strain," *Solid-State Electronics*, vol. 87, pp. 17 – 20, 2013. [Online]. Available: http://www.sciencedirect.com/science/article/pii/S0038110113002001

[19] L. Petti, F. Loghin, G. Cantarella, C. Vogt, N. Münzenrieder, A. Abdellah, M. Becherer, T. Haeberle, A. Daus, G. Salvatore, G. Tröster, and P. Lugli, "Gain-tunable complementary common-source amplifier based on a flexible hybrid thin-film transistor technology," *IEEE Electron Device Letters*, vol. 38, no. 11, pp. 1536–1539, Nov. 2017.

[20] A. Rahaman, H. Jeong, and J. Jang, "A high-gain CMOS operational amplifier using low-temperature poly-Si oxide TFTs," *IEEE Trans. Electron Devices*, vol. 67, no. 2, pp. 524–528, Feb. 2020.

[21] Y. Liang, X. Liang, Z. Zhang, W. Li, X. Huo, and L. Peng, "High mobility flexible graphene field-effect transistors and ambipolar radio-frequency circuits," *Nanoscale*, vol. 7, pp. 10 954–10 962, 2015. [Online]. Available: http://dx.doi.org/10.1039/C5NR02292D

[22] S.-K. Lee, H. Y. Jang, S. Jang, E. Choi, B. H. Hong, J. Lee, S. Park, and J.-H. Ahn, "All graphene-based thin film transistors on flexible plastic substrates," *Nano Lett.*, vol. 12, no. 7, pp. 3472–3476, Jul. 2012. [Online]. Available: https://doi.org/10.1021/nl300948c

[23] E. S. Snow, P. M. Campbell, M. G. Ancona, and J. P. Novak, "High-mobility carbon-nanotube thin-film transistors on a polymeric substrate," *Applied Physics Letters*, vol. 86, no. 3, p. 033105, 2005. [Online]. Available: https://doi.org/10.1063/1.1854721

[24] Y. Kuo, "Thin film transistor technology–past, present, and future," *Interface magazine*, vol. 22, no. 1, pp. 55–61, Jan. 2013. [Online]. Available: https://doi.org/10.1149/2.f06131if

[25] Y. Tarn, P. Ku, H. Hsieh, and L. Lu, "An amorphous-Silicon operational amplifier and its application to a 4-bit digital-to-analog converter," *IEEE J. Solid-State Circuits*, vol. 45, no. 5, pp. 1028–1035, May 2010.

[26] C. sung Chiang, J. Kanicki, and K. Takechi, "Electrical instability of hydrogenated amorphous silicon thin-film transistors for active-matrix liquid-crystal displays," *Japanese Journal of Applied Physics*, vol. 37, no. Part 1, No. 9A, pp. 4704–4710, Sep. 1998. [Online]. Available: https://doi.org/10.1143/jjap.37.4704

[27] C. Lee, N. P. Papadopoulos, M. Sachdev, and W. S. Wong, "Effect of mechanical strain on hydrogenated amorphous silicon thin-film transistors and compensation circuits on flexible substrates," *IEEE Transactions on Electron Devices*, vol. 64, no. 5, pp. 2016–2021, May 2017.

[28] A. Kattamis, I.-C. Cheng, K. Long, J. C. Sturm, and S. Wagner, "Nanocrystalline silicon thin film transistors on optically clear polymer foil substrates," *MRS Online Proceedings Library*, vol. 870, no. 1, p. 27, Dec. 2005. [Online]. Available: https://doi.org/10.1557/PROC-870-H2.7

[29] T.-C. Chang, Y.-C. Tsao, P.-H. Chen, M.-C. Tai, S.-P. Huang, W.-C. Su, and G.-F. Chen, "Flexible low-temperature polycrystalline silicon thin-film transistors," *Materials Today Advances*, vol. 5, p. 100040, 2020. [Online]. Available: http://www.sciencedirect.com/science/article/pii/S2590049819301146

[30] S. Brotherton, J. Ayres, M. Edwards, C. Fisher, C. Glaister, J. Gowers, D. McCulloch, and M. Trainor, "Laser crystallised poly-si tfts for amlcds," *Thin Solid Films*, vol. 337, no. 1, pp. 188 – 195, 1999. [Online]. Available: http://www.sciencedirect.com/science/article/pii/S0040609098011766

[31] A. W. Wang and K. C. Saraswat, "A strategy for modeling of variations due to grain size in polycrystalline thin-film transistors," *IEEE Transactions on Electron Devices*, vol. 47, no. 5, pp. 1035–1043, May 2000.

[32] W. Lin, C. Lin, and S. Liu, "A cbsc second-order sigma-delta modulator in 3 µm ltps-tft technology," in *2009 IEEE Asian Solid-State Circuits Conference*, Nov. 2009, pp. 133–136.

[33] K. Myny, A. K. Tripathi, J. van der Steen, and B. Cobb, "Flexible thin-film nfc tags," *IEEE Communications Magazine*, vol. 53, no. 10, pp. 182–189, Oct. 2015.

[34] S. Gupta, W. T. Navaraj, L. Lorenzelli, and R. Dahiya, "Ultra-thin chips for high-performance flexible electronics," *npj Flexible Electronics*, vol. 2, no. 1, p. 8, Mar. 2018. [Online]. Available: https://doi.org/10.1038/s41528-018-0021-5

[35] D. Schrufer, M. Ellinger, M. P. Jank, L. Frey, R. Weigel, and A. Hagelauer, "Circuits with scaled metal oxide technology for future tolae rf systems," in *2018 48th European Microwave Conference (EuMC)*, Sep. 2018, pp. 737–740. [Online]. Available: https://www.eumwa.org/knowledge-center/EUMW2018/EUMC2018/MC182537.PDF

[36] T. Uemura, T. Matsumoto, K. Miyake, M. Uno, S. Ohnishi, T. Kato, M. Katayama, S. Shinamura, M. Hamada, M.-J. Kang, K. Takimiya, C. Mitsui, T. Okamoto, and J. Takeya, "Split-gate organic field-effect transistors for high-speed operation," *Advanced Materials*, vol. 26, no. 19, pp. 2983–2988, 2014. [Online]. Available: https://onlinelibrary.wiley.com/doi/abs/10.1002/adma.201304976

[37] L. Petti, E. Greco, G. Cantarella, N. Münzenrieder, C. Vogt, and G. Tröster, "Flexible in–ga–zn–o thin-film transistors with sub-300-nm channel lengths defined by two-photon direct laser writing," *IEEE Transactions on Electron Devices*, vol. 65, no. 9, pp. 3796–3802, Sep. 2018.

[38] N. Munzenrieder, P. Voser, L. Petti, C. Zysset, L. Buthe, C. Vogt, G. A. Salvatore, and G. Troster, "Flexible self-aligned double-gate IGZO TFT," *IEEE Electron Device Letters*, vol. 35, no. 1, pp. 69–71, Jan. 2014. [Online]. Available: https://doi.org/10.1109/led.2013.2286319

[39] M. P. Klinger, A. Fischer, F. Kaschura, R. Scholz, B. Lüssem, B. Kheradmand-Boroujeni, F. Ellinger, D. Kasemann, and K. Leo, "Advanced organic permeable-base transistor with superior performance," *Advanced Materials*, vol. 27, no. 47, pp. 7734–7739, 2015. [Online]. Available: https://onlinelibrary.wiley.com/doi/abs/10.1002/adma.201502788

[40] H.-R. Kim, M. Furuta, and S.-M. Yoon, "Highly robust flexible vertical-channel thin-film transistors using atomic-layer-deposited oxide channels and zeocoat spacers on ultrathin polyimide substrates," *ACS Applied Electronic Materials*, vol. 1, no. 11, pp. 2363–2370, Oct. 2019. [Online]. Available: https://doi.org/10.1021/acsaelm.9b00544

[41] L. Petti, A. Frutiger, N. Munzenrieder, G. A. Salvatore, L. Buthe, C. Vogt, G. Cantarella, and G. Troster, "Flexible quasi-vertical in-ga-zn-o thin-film transistor with 300-nm channel length," *IEEE Electron Device Letters*, vol. 36, no. 5, pp. 475–477, May 2015. [Online]. Available: https://doi.org/10.1109/led.2015.2418295

[42] N. Münzenrieder, I. Shorubalko, L. Petti, G. Cantarella, B. Shkodra, T. Meister, K. Ishida, C. Carta, F. Ellinger, and G. Tröster, "Focused ion beam milling for the fabrication of 160 nm channel length IGZO TFTs on flexible polymer substrates," *Flexible and Printed Electronics*, vol. 5, no. 1, p. 015007, Jan. 2020. [Online]. Available: https://doi.org/10.1088/2058-8585/ab639f

[43] J. W. Borchert, U. Zschieschang, F. Letzkus, M. Giorgio, M. Caironi, J. N. Burghartz, S. Ludwigs, and H. Klauk, "Record static and dynamic performance of flexible organic thin-film transistors," in *2018*

IEEE International Electron Devices Meeting (IEDM), Dec. 2018, pp. 38.4.1–38.4.4.

[44] A. Yamamura, S. Watanabe, M. Uno, M. Mitani, C. Mitsui, J. Tsurumi, N. Isahaya, Y. Kanaoka, T. Okamoto, and J. Takeya, "Wafer-scale, layer-controlled organic single crystals for high-speed circuit operation," *Science Advances*, vol. 4, no. 2, 2018. [Online]. Available: https://advances.sciencemag.org/content/4/2/eaao5758

[45] A. Perinot, P. Kshirsagar, M. A. Malvindi, P. P. Pompa, R. Fiammengo, and M. Caironi, "Direct-written polymer field-effect transistors operating at 20 mhz," *Scientific Reports*, vol. 6, no. 1, p. 38941, Dec. 2016. [Online]. Available: https://doi.org/10.1038/srep38941

[46] K. Nakayama, M. Uno, T. Uemura, N. Namba, Y. Kanaoka, T. Kato, M. Katayama, C. Mitsui, T. Okamoto, and J. Takeya, "High-mobility organic transistors with wet-etch-patterned top electrodes: A novel patterning method for fine-pitch integration of organic devices," *Advanced Materials Interfaces*, vol. 1, no. 5, p. 1300124, 2014. [Online]. Available: https://onlinelibrary.wiley.com/doi/abs/10.1002/admi.201300124

[47] J. Sheng, T. Hong, H.-M. Lee, K. Kim, M. Sasase, J. Kim, H. Hosono, and J.-S. Park, "Amorphous IGZO TFT with high mobility of $\sim$70 cm2/(v s) via vertical dimension control using PEALD," *ACS Applied Materials & Interfaces*, vol. 11, no. 43, pp. 40 300–40 309, Oct. 2019. [Online]. Available: https://doi.org/10.1021/acsami.9b14310

[48] L. Petti, E. Greco, G. Cantarella, N. Munzenrieder, C. Vogt, and G. Troster, "Flexible in–ga–zn–o thin-film transistors with sub-300-nm channel lengths defined by two-photon direct laser writing," *IEEE Transactions on Electron Devices*, vol. 65, no. 9, pp. 3796–3802, Sep. 2018. [Online]. Available: https://doi.org/10.1109/ted.2018.2851926

[49] R. Yao, Z. Zheng, Z. Fang, H. Zhang, X. Zhang, H. Ning, L. Wang, J. Peng, W. Xie, and X. Lu, "High-performance flexible oxide TFTs: optimization of a-IGZO film by modulating the voltage waveform of pulse DC magnetron sputtering without post treatment," *Journal of Materials Chemistry C*, vol. 6, no. 10, pp. 2522–2532, 2018. [Online]. Available: https://doi.org/10.1039/c7tc04970f

[50] J. Kim, J. Jang, Y. Kim, J. Byun, K. Han, J. Park, and B. Choi, "Dynamic logic circuits using a-igzo tfts," *IEEE Trans. Electron Devices*, vol. 64, no. 10, pp. 4123–4130, Oct. 2017.

[51] M. Nag, F. De Roose, K. Myny, S. Steudel, J. Genoe, G. Groeseneken, and P. Heremans, "Characteristics improvement of top-gate self-aligned amorphous indium gallium zinc oxide thin-film transistors using a dual-gate control," *Journal of the Society for Information Display*, vol. 25, no. 6, pp. 349–355, 2017. [Online]. Available: https://onlinelibrary.wiley.com/doi/abs/10.1002/jsid.558

[52] M. Mativenga, D. Geng, B. Kim, and J. Jang, "Fully transparent and rollable electronics," *ACS Appl. Mater. Interfaces*, vol. 7, no. 3, pp. 1578–1585, Jan. 2015. [Online]. Available: https://doi.org/10.1021/am506937s

[53] M. Nag, K. Obata, Y. Fukui, K. Myny, S. Schols, P. Vicca, T. H. Ke, S. Smout, M. Willegems, M. Ameys, A. Bhoolokam, R. Muller, B. Cobb, A. Kumar, J.-L. van der Steen, T. Ellis, G. Gelinck, J. Genoe, P. Heremans, and S. Steudel, "20.1: Flexible amoled display and gate-driver with self-aligned igzo tft on plastic foil," *SID Symposium Digest of Technical Papers*, vol. 45, no. 1, pp. 248–251, 2014. [Online]. Available: https://onlinelibrary.wiley.com/doi/abs/10.1002/j.2168-0159.2014.tb00068.x

[54] N. Munzenrieder, L. Petti, C. Zysset, T. Kinkeldei, G. A. Salvatore, and G. Troster, "Flexible self-aligned amorphous InGaZnO thin-film transistors with submicrometer channel length and a transit frequency of 135 MHz," *IEEE Transactions on Electron Devices*, vol. 60, no. 9, pp. 2815–2820, Sep. 2013. [Online]. Available: https://doi.org/10.1109/ted.2013.2274575

[55] N. Münzenrieder, L. Petti, C. Zysset, G. A. Salvatore, T. Kinkeldei, C. Perumal, C. Carta, F. Ellinger, and G. Tröster, "Flexible a-IGZO TFT amplifier fabricated on a free standing polyimide foil operating at 1.2 MHz while bent to a radius of 5 mm," in *2012 International Electron Devices Meeting*, Dec. 2012, pp. 5.2.1–5.2.4.

[56] X. Wei, S. Kumagai, K. Tsuzuku, A. Yamamura, T. Makita, M. Sasaki, S. Watanabe, and J. Takeya, "Solution-processed flexible metal-oxide thin-film transistors operating beyond 20 MHz," *Flexible and Printed Electronics*, vol. 5, no. 1, p. 015003, Jan. 2020. [Online]. Available: https://doi.org/10.1088/2058-8585/ab603b

[57] M. Wang, X. Li, X. Xiong, J. Song, C. Gu, D. Zhan, Q. Hu, S. Li, and Y. Wu, "High-performance flexible ZnO thin-film transistors by atomic layer deposition," *IEEE Electron Device Letters*, vol. 40, no. 3, pp. 419–422, Mar. 2019. [Online]. Available: https://doi.org/10.1109/led.2019.2895864

[58] D. Han, Y. Zhang, Y. Cong, W. Yu, X. Zhang, and Y. Wang, "Fully transparent flexible tin-doped zinc oxide thin film transistors fabricated on plastic substrate," *Scientific Reports*, vol. 6, no. 1, p. 38984, Dec. 2016. [Online]. Available: https://doi.org/10.1038/srep38984

[59] H. Kim, D. Y. Jeong, S. Lee, and J. Jang, "A high-gain inverter with low-temperature poly-si oxide thin-film transistors," *IEEE Electron Device Letters*, vol. 40, no. 3, pp. 411–414, Mar. 2019.

[60] G. Jin, J. Choi, W. Lee, Y. Mo, H. Kim, S. Kim, M. Kim, and J. Song, "Simple fabrication of a three-dimensional cmos inverter using p-type poly-si and n-type amorphous ga–in–zn–o thin-film transistors," *IEEE Electron Device Letters*, vol. 32, no. 9, pp. 1236–1238, Sep. 2011.

[61] C. Chen, B. Yang, C. Liu, X. Zhou, Y. Hsu, Y. Wu, J. lm, P. Lu, M. Wong, H. Kwok, and H. D. Shieh, "Integrating poly-silicon and ingazno thin-film transistors for cmos inverters," *IEEE Transactions on Electron Devices*, vol. 64, no. 9, pp. 3668–3671, Sep. 2017.

[62] K. M. Lim, K. Lee, J. S. Yoo, J.-M. Yoon, M. K. Baek, J.-S. Yoo, Y.-S. Jung, J. Park, S.-W. Lee, H. Kang, C.-D. Kim, and I.-J. Chung, "A 3.5in. qvga poly-si tft-lcd with integrated driver including new 6-bit dac," *Solid-State Electronics*, vol. 49, no. 7, pp. 1107 – 1111, 2005. [Online]. Available: http://www.sciencedirect.com/science/article/pii/S003811010500136X

[63] S.-J. Kim, S.-M. Han, and M.-K. Han, "Nanocrystalline silicon thin-film transistor fabricated without substrate heating for flexible display," *Japanese Journal of Applied Physics*, vol. 48, no. 8, p. 081202, Aug. 2009. [Online]. Available: https://doi.org/10.1143/jjap.48.081202

[64] C.-H. Lee, A. Sazonov, A. Nathan, and J. Robertson, "Directly deposited nanocrystalline silicon thin-film transistors with ultra high mobilities," *Applied Physics Letters*, vol. 89, no. 25, p. 252101, 2006. [Online]. Available: https://doi.org/10.1063/1.2408630

[65] I. Chiu, J. Huang, Y. Chen, I. Cheng, J. Z. Chen, and M. Lee, "Electromechanical stability of flexible nanocrystalline-silicon thin-film transistors," *IEEE Electron Device Letters*, vol. 31, no. 3, pp. 222–224, Mar. 2010.

[66] C. C. Chiang, D. S. Wuu, Y. P. Chen, T. H. Jaw, and R. H. Horng, "Fabrication of amorphous si thin-film transistors on an engineered parylene template using a direct separation process," *Electrochemical and Solid-State Letters*, vol. 11, no. 1, p. J4, 2008. [Online]. Available: https://doi.org/10.1149%2F1.2805080

[67] S. Noyce, J. L. Doherty, Z. Cheng, H. Han, S. Bowen, and A. D. Franklin, "Electronic stability of carbon nanotube transistors under long-term bias stress," *Nano Lett.*, vol. 19, no. 3, pp. 1460–1466, Mar. 2019. [Online]. Available: https://doi.org/10.1021/acs.nanolett.8b03986

[68] T. Lei, L.-L. Shao, Y.-Q. Zheng, G. Pitner, G. Fang, C. Zhu, S. Li, R. Beausoleil, H.-S. P. Wong, T.-C. Huang, K.-T. Cheng, and Z. Bao, "Low-voltage high-performance flexible digital and analog circuits based on ultrahigh-purity semiconducting carbon nanotubes," *Nature Communications*, vol. 10, no. 1, p. 2161, May 2019. [Online]. Available: https://doi.org/10.1038/s41467-019-10145-9

[69] J. Tang, Q. Cao, G. Tulevski, K. A. Jenkins, L. Nela, D. B. Farmer, and S.-J. Han, "Flexible cmos integrated circuits based on carbon nanotubes with sub-10 ns stage delays," *Nature Electronics*, vol. 1, no. 3, pp. 191–196, Mar. 2018. [Online]. Available: https://doi.org/10.1038/s41928-018-0038-8

[70] S. P. Schießl, N. Fröhlich, M. Held, F. Gannott, M. Schweiger, M. Forster, U. Scherf, and J. Zaumseil, "Polymer-sorted semiconducting carbon nanotube networks for high-performance ambipolar field-effect transistors," *ACS Appl. Mater. Interfaces*, vol. 7, no. 1, pp. 682–689, Jan. 2015. [Online]. Available: https://doi.org/10.1021/am506971b

[71] Y. Zhu, Y. He, S. Jiang, L. Zhu, C. Chen, and Q. Wan, "Indium-gallium-zinc-oxide thin-film transistors: Materials, devices, and applications," *Journal of Semiconductors*, vol. 42, no. 3, p. 031101, Mar. 2021. [Online]. Available: https://doi.org/10.1088/1674-4926/42/3/031101

[72] G. Cantarella, J. Costa, T. Meister, K. Ishida, C. Carta, F. Ellinger, P. Lugli, N. Münzenrieder, and L. Petti, "Review of recent trends in flexible metal oxide thin-film transistors for analog applications," *Flexible and Printed Electronics*, vol. 5, no. 3, p. 033001, Jul. 2020.

[73] L. Xiang, X. Zeng, F. Xia, W. Jin, Y. Liu, and Y. Hu, "Recent advances in flexible and stretchable sensing systems: From the perspective of system integration," *ACS Nano*, vol. 14, no. 6, pp. 6449–6469, Jun. 2020. [Online]. Available: https://doi.org/10.1021/acsnano.0c01164

[74] A. J. Kronemeijer, I. Katsouras, P. Poodt, H. Akkerman, A. Van Breemen, and G. Gelinck, "Flexible a-igzo tft technology: New developments & applications," in *2018 25th International Workshop on Active-Matrix Flatpanel Displays and Devices (AM-FPD)*, Jul. 2018, pp. 1–4.

[75] K. Myny, "The development of flexible integrated circuits based on thin-film transistors," *Nature Electronics*, vol. 1, no. 1, pp. 30–39, Jan. 2018. [Online]. Available: https://doi.org/10.1038/s41928-017-0008-6

[76] J. Y. Choi and S. Y. Lee, "Comprehensive review on the development of high mobility in oxide thin film transistors," *Journal of the Korean Physical Society*, vol. 71, no. 9, pp. 516–527, Nov. 2017. [Online]. Available: https://doi.org/10.3938/jkps.71.516

[77] G. A. Salvatore, "Soft and bio-degradable electronics: Technology challenges and future applications," in *2016 46th European Solid-State Device Research Conference (ESSDERC)*, Sep. 2016, pp. 381–384.

[78] K. Myny, S. Steudel, P. Vicca, M. J. Beenhakkers, N. A. van Aerle, G. H. Gelinck, J. Genoe, W. Dehaene, and P. Heremans, "Plastic circuits and tags for 13.56mhz radio-frequency communication," *Solid-State Electronics*, vol. 53, no. 12, pp. 1220 – 1226, 2009, papers Selected from the Ultimate Integration on Silicon Conference 2009, ULIS 2009.

[79] L. Zhang, W. Xiao, W. Wu, and B. Liu, "Research progress on flexible oxide-based thin film transistors," *Applied Sciences*, vol. 9, no. 4, p. 773, 2019. [Online]. Available: https://doi.org/10.3390/app9040773

[80] M. S. Shur, H. C. Slade, M. D. Jacunski, A. A. Owusu, and T. Ytterdal, "SPICE models for amorphous silicon and polysilicon thin film transistors," *Journal of The Electrochemical Society*, vol. 144, no. 8, pp. 2833–2839, Aug. 1997. [Online]. Available: https://doi.org/10.1149/1.1837903

[81] O. Marinov, M. J. Deen, U. Zschieschang, and H. Klauk, "Organic thin-film transistors: Part i—compact dc modeling," *IEEE Transactions on Electron Devices*, vol. 56, no. 12, pp. 2952–2961, Dec. 2009.

[82] M. J. Deen, O. Marinov, U. Zschieschang, and H. Klauk, "Organic thin-film transistors: Part ii—parameter extraction," *IEEE Transactions on Electron Devices*, vol. 56, no. 12, pp. 2962–2968, Dec. 2009.

[83] O. Marinov and M. Jamal Deen, "Quasistatic compact modelling of organic thin-film transistors," *Organic Electronics*, vol. 14, no. 1, pp. 295 – 311, 2013. [Online]. Available: http://www.sciencedirect.com/science/article/pii/S1566119912004971

[84] Zhiwei Zong, Ling Li, Jin Jang, Zhigang Li, Nianduan Lu, Liwei Shang, Zhuoyu Ji, and Ming Liu, "A new surface potential-based compact model for a-igzo tfts in rfid applications," in *2014 IEEE International Electron Devices Meeting*, Dec. 2014, pp. 35.5.1–35.5.4.

[85] C. Perumal, K. Ishida, R. Shabanpour, B. K. Boroujeni, L. Petti, N. S. Münzenrieder, G. A. Salvatore, C. Carta, G. Tröster, and F. Ellinger, "A compact a-IGZO TFT model based on MOSFET SPICE $\mathrm{level} = 3$ template for analog/rf circuit designs," *IEEE Electron Device Lett.*, vol. 34, no. 11, pp. 1391–1393, Nov. 2013.

[86] R. Shabanpour, T. Meister, K. Ishida, B. Boroujeni, C. Carta, F. Ellinger, L. Petti, N. Münzenrieder, G. A. Salvatore, and G. Tröster, "A transistor model for a-igzo tft circuit design built upon the rpi-atft model," in *2017 15th IEEE International New Circuits and Systems Conference (NEWCAS)*, Jun. 2017, pp. 129–132.

[87] T. Huang, L. Shao, T. Lei, R. Beausoleil, Z. Bao, and K. Cheng, "Robust design and design automation for flexible hybrid electronics," in *2017 IEEE International Symposium on Circuits and Systems (ISCAS)*, May 2017, pp. 1–4.

[88] C. D. Holdenried, M. W. Lynch, and J. W. Haslett, "Modified cmos cherry-hooper amplifiers with source follower feedback in 0.35/spl mu/m technology," in *ESSCIRC 2004 - 29th European Solid-State Circuits Conference (IEEE Cat. No.03EX705)*, Sep. 2003, pp. 553–556.

[89] T. Huang, K. Fukuda, C. Lo, Y. Yeh, T. Sekitani, T. Someya, and K. Cheng, "Pseudo-cmos: A design style for low-cost and robust flexible electronics," *IEEE Transactions on Electron Devices*, vol. 58, no. 1, pp. 141–150, Jan. 2011.

[90] K. Ishida, R. Shabanpour, T. Meister, B. K. Boroujeni, C. Carta, L. Petti, N. Münzenrieder, G. A. Salvatore, G. Tröster, and F. Ellinger, "15 db conversion gain, 20 mhz carrier frequency am receiver in flexible a-igzo tft technology with textile antennas," in *2015 Symposium on VLSI Circuits (VLSI Circuits)*, Jun. 2015, pp. C194–C195.

[91] K. Ishida, R. Shabanpour, T. Meister, B. K. Boroujeni, C. Carta, F. Ellinger, L. Petti, N. Münzenrieder, G. A. Salvatore, and G. Tröster, "20 mhz carrier frequency am receiver in flexible a-igzo tft technology with textile antennas," in *2015 IEEE International Symposium on Radio-Frequency Integration Technology (RFIT)*, Aug. 2015, pp. 142–144.

[92] T. Meister, K. Ishida, A. Sou, C. Carta, and F. Ellinger, "49.35 mhz gbw and 33.43 mhz gbw amplifiers in flexible a-igzo tft technology," *Electronics Letters*, vol. 56, pp. 782–785(3), Jul. 2020. [Online]. Available: https://digital-library.theiet.org/content/journals/10.1049/el.2020.0813

[93] Z. Chen, W. Xu, J. Wu, L. Zhou, W. Wu, J. Zou, M. Xu, L. Wang, Y. Liu, and J. Peng, "A new high-gain operational amplifier using transconductance-enhancement topology integrated with metal oxide TFTs," *IEEE Journal of the Electron Devices Society*, vol. 7, no. 1, pp. 111–117, 2019.

[94] A. Rahaman, Y. Chen, M. M. Hasan, and J. Jang, "A high performance operational amplifier using coplanar dual gate a-IGZO TFTs," *IEEE Journal of the Electron Devices Society*, vol. 7, no. 1, pp. 655–661, 2019.

[95] P. G. Bahubalindruni, J. Martins, A. Santa, V. Tavares, R. Martins, E. Fortunato, and P. Barquinha, "High-gain transimpedance amplifier for flexible radiation dosimetry using ingazno tfts," *IEEE Journal of the Electron Devices Society*, vol. 6, pp. 760–765, 2018.

[96] C. Garripoli, S. Abdinia, J. J. P. van der Steen, G. H. Gelinck, and E. Cantatore, "A fully integrated 11.2-mm2 a-igzo emg front-end circuit on flexible substrate achieving up to 41-db snr and 29-m ω input impedance," *IEEE Solid-State Circuits Letters*, vol. 1, no. 6, pp. 142–145, Jun. 2018.

[97] M. Zulqarnain, S. Stanzione, J. P. J. Van Der Steen, G. H. Gelinck, K. Myny, S. Abdinia, and E. Cantatore, "A 52 µw heart-rate measurement interface fabricated on a flexible foil with a-igzo tfts," in *ESSCIRC 2018 - IEEE 44th European Solid State Circuits Conference (ESSCIRC)*, Sep. 2018, pp. 222–225.

[98] C. Garripoli, J. P. J. van der Steen, F. Torricelli, M. Ghittorelli, G. H. Gelinck, A. H. M. Van Roermund, and E. Cantatore, "Analogue frontend amplifiers for bio-potential measurements manufactured with a-igzo tfts on flexible substrate," *IEEE Journal on Emerging and Selected Topics in Circuits and Systems*, vol. 7, no. 1, pp. 60–70, Mar. 2017.

[99] K. Kim, K. Choi, and H. Lee, "a-InGaZnO thin-film transistor-based operational amplifier for an adaptive dc–dc converter in display driving systems," *IEEE Trans. Electron Devices*, vol. 62, no. 4, pp. 1189–1194, Apr. 2015.

[100] R. Shabanpour, K. Ishida, T. Meister, N. Munzenrieder, L. Petti, G. Salvatore, B. Kheradmand-Boroujeni, C. Carta, G. Troster, and F. Ellinger, "A 70°phase margin opamp with positive feedback in flexible a-igzo tft technology," in *Circuits and Systems (MWSCAS), 2015 IEEE 58th International Midwest Symposium on*, Aug. 2015, pp. 1–4.

[101] R. Shabanpour, T. Meister, K. Ishida, L. Petti, N. Münzenrieder, G. A. Salvatore, B. K. Boroujeni, C. Carta, G. Tröster, and F. Ellinger, "High gain amplifiers in flexible self-aligned a-IGZO thin-film-transistor technology," in *2014 21st IEEE International Conference on Electronics, Circuits and Systems (ICECS)*, Dec. 2014, pp. 108–111.

[102] R. Shabanpour, T. Meister, K. Ishida, B. Kheradmand Boroujeni, C. Carta, U. Jörges, F. Ellinger, L. Petti, N. Münzenrieder, G. A. Salvatore, and G. Tröster, "Cherry-Hooper amplifiers with 33 dB gain at 400 kHz BW and 10 dB gain at 3.5 MHz BW in flexible self-aligned a-IGZO TFT technology," in *2014 International Symposium on Intelligent Signal Processing and Communication Systems (ISPACS)*, Dec. 2014, pp. 271–274.

[103] K. Ishida, R. Shabanpour, B. K. Boroujeni, T. Meister, C. Carta, F. Ellinger, L. Petti, N. S. Munzenrieder, G. A. Salvatore, and G. Troster, "22.5 db open-loop gain, 31 khz gbw pseudo-cmos based operational amplifier with a-igzo tfts on a flexible film," in *Solid-State Circuits Conference (A-SSCC), 2014 IEEE Asian*, 2014, pp. 313–316.

[104] C. Zysset, N. Münzenrieder, L. Petti, L. Büthe, G. A. Salvatore, and G. Tröster, "Igzo tft-based all-enhancement operational amplifier bent to a radius of 5 mm," *IEEE Electron Device Letters*, vol. 34, no. 11, pp. 1394–1396, Nov. 2013.

[105] Y. Chen, D. Geng, M. Mativenga, H. Nam, and J. Jang, "High-speed pseudo-CMOS circuits using bulk accumulation a-IGZO TFTs," *IEEE Electron Device Letters*, vol. 36, no. 2, pp. 153–155, Feb. 2015.

[106] F. De Roose, J. Genoe, W. Dehaene, and K. Myny, "Crossover logic: A low-power topology for unipolar dual-gate thin-film technologies," *IEEE Solid-State Circuits Letters*, vol. 2, no. 7, pp. 49–52, Jul. 2019.

[107] K. Ishida, T. Meister, S. Knobelspies, N. Münzenrieder, G. Cantarella, G. A. Salvatore, G. Tröster, C. Carta, and F. Ellinger, "3–5 V, 3–3.8 MHz OOK modulator with a-IGZO TFTs for flexible wireless transmitter," in *2017 IEEE COMCAS*, Nov. 2017, pp. 1–4.

[108] Y. Chen, D. Geng, T. Lin, M. Mativenga, and J. Jang, "Full-swing clock generating circuits on plastic using a-igzo dual-gate tfts with pseudo-cmos and bootstrapping," *IEEE Electron Device Letters*, vol. 37, no. 7, pp. 882–885, Jul. 2016.

[109] K. Myny and S. Steudel, "Flexible thin-film NFC transponder chip exhibiting data rates compatible to ISO NFC standards using self-

aligned metal-oxide TFTs," in *2016 IEEE International Solid-State Circuits Conference (ISSCC)*, Jan. 2016, pp. 298–299.

[110] T. Meister, K. Ishida, R. Shabanpour, B. K. Boroujeni, C. Carta, N. Münzenrieder, L. Petti, G. A. Salvatore, G. Tröster, M. Wagner, P. Ghesquiere, S. Kiefl, M. Krebs, and F. Ellinger, "Bendable energy-harvesting module with organic photovoltaic, rechargeable battery, and a-IGZO TFT charging electronics," in *22nd European conference on circuit theory and design, ECCTD2015*, Trondheim, Aug. 2015.

[111] X. Li, D. Geng, M. Mativenga, and J. Jang, "High-speed dual-gate a-IGZO TFT-based circuits with top-gate offset structure," *IEEE Electron Device Letters*, vol. 35, no. 4, pp. 461–463, Apr. 2014.

[112] B.-D. Yang, J.-M. Oh, H.-J. Kang, S.-H. Park, C.-S. Hwang, M. K. Ryu, and J.-E. Pi, "A transparent logic circuit for RFID tag in a-IGZO TFT technology," *ETRI Journal*, vol. 35, no. 4, pp. 610–616, Aug. 2013. [Online]. Available: https://onlinelibrary.wiley.com/doi/abs/10.4218/etrij.13.1912.0004

[113] M. Mativenga, M. H. Choi, J. W. Choi, and J. Jang, "Transparent flexible circuits based on amorphous-indium-gallium-zinc-oxide thin-film transistors," *IEEE Electron Device Letters*, vol. 32, no. 2, pp. 170–172, Feb. 2011.

[114] D. H. Kang, I. Kang, S. H. Ryu, and J. Jang, "Self-aligned coplanar a-igzo tfts and application to high-speed circuits," *IEEE Electron Device Letters*, vol. 32, no. 10, pp. 1385–1387, Oct. 2011.

[115] A. Suresh, P. Wellenius, V. Baliga, H. Luo, L. M. Lunardi, and J. F. Muth, "Fast all-transparent integrated circuits based on indium gallium zinc oxide thin-film transistors," *IEEE Electron Device Letters*, vol. 31, no. 4, pp. 317–319, Apr. 2010.

[116] J. D. Wu, F. Zhan, L. Zhou, W. J. Wu, M. Xu, L. Wang, R. H. Yao, J. B. Peng, and M. Chan, "A low-power ring oscillator using pull-up control scheme integrated by metal-oxide tfts," *IEEE Transactions on Electron Devices*, vol. 64, no. 12, pp. 4946–4951, Dec. 2017.

[117] J. H. Na, M. Kitamura, and Y. Arakawa, "Organic/inorganic hybrid complementary circuits based on pentacene and amorphous indium gallium zinc oxide transistors," *Applied Physics Letters*, vol. 93, no. 21, p. 213505, 2008. [Online]. Available: https://doi.org/10.1063/1.3039779

[118] T. C. Huang and K. T. Cheng, "Design for low power and reliable flexible electronics: Self-tunable cell-library design," *Journal of Display Technology*, vol. 5, no. 6, pp. 206–215, Jun. 2009.

[119] H. Fuketa, M. Hamamatsu, T. Yokota, W. Yukita, T. Someya, T. Sekitani, M. Takamiya, T. Someya, and T. Sakurai, "Energy-autonomous fever alarm armband integrating fully flexible solar cells, piezoelectric speaker, temperature detector, and 12V organic complementary FET circuits," in *2015 IEEE International Solid-State Circuits Conference - (ISSCC) Digest of Technical Papers*, Feb. 2015, pp. 1–3.

[120] G. C. Schmidt, D. Höft, K. Haase, M. Bellmann, B. Kheradmand-Boroujeni, T. Hassinen, H. Sandberg, F. Ellinger, and A. C. Hübler, "Fully printed flexible audio system on the basis of low-voltage polymeric organic field effect transistors with three layer dielectric," *Journal of Polymer Science Part B: Polymer Physics*, vol. 53, no. 20, pp. 1409–1415, Jul. 2015. [Online]. Available: https://onlinelibrary.wiley.com/doi/abs/10.1002/polb.23778

[121] T. Meister, F. Ellinger, J. W. Bartha, M. Berroth, J. Burghartz, M. Claus, L. Frey, A. Gagliardi, M. Grundmann, J. Hesselbarth, H. Klauk, K. Leo, P. Lugli, S. Mannsfeld, Y. Manoli, R. Negra, D. Neumaier, U. Pfeiffer, T. Riedl, S. Scheinert, U. Scherf, A. Thiede, G. Tr öster, M. Vossiek, R. Weigel, C. Wenger, G. Alavi, M. Becherer, C. A. Chavarin, M. Darwish, M. Ellinger, C.-Y. Fan, M. Fritsch, F. Grotjahn, M. Gunia, K. Haase, P. Hillger, K. Ishida, M. Jank, S. Knobelspies, M. Kuhl, G. Lupina, S. M. Naghadeh, N. M ünzenrieder, S. Ö, M. Rasteh, G. Salvatore, D. Schr üfer, C. Strobel, M. Theisen, C. T ückmantel, H. von Wenckstern, Z. Wang, and Z. Zhipeng, "Program fflexcom - high frequency flexible bendable electronics for wireless communication systems," in *2017 IEEE International Conference on Microwave, Communications, Antennas and Electronic Systems (COMCAS 2017)*, Tel Aviv, Israel, Nov. 2017, pp. 1–6. [Online]. Available: https://publications.meistertilo.de/wp-content/uploads/2018/08/171115_COMCAS_FFlexComOverview.pdf

[122] C.-Y. Fan, R. Negra, M.-D. Wei, M. Saeed, A. H. Ghareeb, Z. Wang, M. Shaygan, and D. Neumaier, "Study of Graphene Flexible Electronics for Microwave Applications," in *[48th European Microwave Conference, EuMC2018, 2018-09-25 - 2018-09-27, Madrid, Spain]*. 48th European Microwave Conference, Madrid (Spain), 25 Sep 2018 - 27 Sep 2018, Sep. 2018, pp. 1–4. [Online]. Available: https://publications.rwth-aachen.de/record/759817

[123] S. Özbek, J. Digel, M. Grözing, M. Berroth, G. Alavi, and J. N. Burghartz, "3-path 5–6 ghz 0.25 μm sige bicmos power amplifier on thin substrate," in *2017 13th Conference on Ph.D. Research in Microelectronics and Electronics (PRIME)*, Jun. 2017, pp. 49–52.

[124] T. Meister, K. Ishida, R. Shabanpour, B. K. Boroujeni, C. Carta, N. Münzenrieder, L. Petti, G. Cantarella, G. A. Salvatore, G. Tröster, and F. Ellinger, "20.3db 0.39mw am detector with single-transistor active inductor in bendable a-igzo tft," in *ESSCIRC Conference 2016: 42nd European Solid-State Circuits Conference*, Sep. 2016, pp. 79–82.

[125] K. Myny, M. J. Beenhakkers, N. A. J. M. van Aerle, G. H. Gelinck, J. Genoe, W. Dehaene, and P. Heremans, "A 128b organic rfid transponder chip, including manchester encoding and aloha anti-collision protocol, operating with a data rate of 1529b/s," in *2009 IEEE International Solid-State Circuits Conference - Digest of Technical Papers*, Feb. 2009, pp. 206–207.

[126] K. Myny, M. Rockelé, A. Chasin, D. Pham, J. Steiger, S. Botnaras, D. Weber, B. Herold, J. Ficker, B. van der Putten, G. Gelinck, J. Genoe, W. Dehaene, and P. Heremans, "Bidirectional communication in an hf hybrid organic/solution-processed metal-oxide rfid tag," in *2012 IEEE International Solid-State Circuits Conference*, Feb. 2012, pp. 312–314.

[127] V. Fiore, P. Battiato, S. Abdinia, S. Jacobs, I. Chartier, R. Coppard, G. Klink, E. Cantatore, E. Ragonese, and G. Palmisano, "An integrated 13.56-mhz rfid tag in a printed organic complementary tft technology on flexible substrate," *IEEE Transactions on Circuits and Systems I: Regular Papers*, vol. 62, no. 6, pp. 1668–1677, Jun. 2015.

[128] E. Cantatore, T. C. T. Geuns, G. H. Gelinck, E. van Veenendaal, A. F. A. Gruijthuijsen, L. Schrijnemakers, S. Drews, and D. M. de Leeuw, "A 13.56-mhz rfid system based on organic transponders," *IEEE Journal of Solid-State Circuits*, vol. 42, no. 1, pp. 84–92, Jan. 2007.

[129] K. Myny, Y. Lai, N. Papadopoulos, F. De Roose, M. Ameys, M. Willegems, S. Smout, S. Steudel, W. Dehaene, and J. Genoe, "15.2 a flexible iso14443-a compliant 7.5mw 128b metal-oxide nfc barcode tag with direct clock division circuit from 13.56mhz carrier," in *2017 IEEE International Solid-State Circuits Conference (ISSCC)*, Feb. 2017, pp. 258–259.

[130] N. Papadopoulos, S. Smout, M. Willegems, M. Nag, M. Ameys, and K. Myny, "2-d smart surface object localization by flexible 160-nw monolithic capacitively coupled 12-b identification tags based on metal–oxide tfts," *IEEE Transactions on Electron Devices*, vol. 65, no. 11, pp. 4861–4867, Nov. 2018.

[131] N. Papadopoulos, S. Smout, M. Willegems, M. Ameys, G. Rathinavel, G. Beeckman, J. Stuijt, and K. Myny, "1cm2 sub-1v capacitive-coupled thin film id-tag using metal-oxide tfts on flexible substrate," in *2018 International Flexible Electronics Technology Conference (IFETC)*, Aug. 2018, pp. 1–2.

[132] K. Myny, B. Cobb, J. van der Steen, A. K. Tripathi, J. Genoe, G. Gelinck, and P. Heremans, "16.3 flexible thin-film nfc tags powered by commercial usb reader device at 13.56mhz," in *2015 IEEE International Solid-State Circuits Conference - (ISSCC) Digest of Technical Papers*, Feb. 2015, pp. 1–3.

[133] Y. Qin, G. Li, Y. Xu, R. Chen, S. Deng, W. Zhong, Z. Wu, B. Li, G. Li, F. S. Y. Yeung, M. Wong, and H. S. Kwok, "Low-power design for unipolar ito-stabilized zno tft rfid code generator using differential logic decoder," *IEEE Transactions on Electron Devices*, vol. 66, no. 11, pp. 4768–4773, Nov. 2019.

[134] H. Xu, Z. Ye, N. Liu, Y. Wang, N. Zhang, and Y. Liu, "Low-power transparent rfid circuits using enhancement/depletion logic gates based on deuterium-treated zno tfts," *IEEE Electron Device Letters*, vol. 38, no. 10, pp. 1383–1386, Oct. 2017.

[135] Ming-Hao Hung, Chung-Hung Chen, Yi-Cheng Lai, Kuan-Wen Tung, Wei-Ting Lin, Hsiu-Hua Wang, Feng-Jui Chan, Chun-Cheng Cheng, Chin-Tang Chuang, Yu-Sheng Huang, Cheng-Nan Yeh, Chu-Yu Liu, Jen-Pei Tseng, Min-Feng Chiang, and Yu-Chieh Lin, "Ultra low voltage 1-v rfid tag implement in a-igzo tft technology on plastic," in *2017 IEEE International Conference on RFID (RFID)*, May 2017, pp. 193–197.

[136] K. M. Gee, P. Anandarajah, and D. Collins, "A review of chipless remote sensing solutions based on rfid technology," *Sensors (Basel, Switzerland)*, vol. 19, 2019.

[137] T. Meister, K. Ishida, S. Knobelspies, G. Cantarella, N. Münzenrieder, G. Tröster, C. Carta, and F. Ellinger, "5–31-hz 188- μ w light-sensing oscillator with two active inductors fully integrated on plastic," *IEEE Journal of Solid-State Circuits*, vol. 54, no. 8, pp. 2195–2206, Aug. 2019.

[138] H. Fuketa, K. Yoshioka, T. Yokota, W. Yukita, M. Koizumi, M. Sekino, T. Sekitani, M. Takamiya, T. Someya, and T. Sakurai, "30.3 organic-transistor-based 2kv esd-tolerant flexible wet sensor sheet for biomedical applications with wireless power and data transmission using 13.56mhz magnetic resonance," in *2014 IEEE International Solid-State*

Circuits Conference Digest of Technical Papers (ISSCC), Feb. 2014, pp. 490–491.

[139] K. Myny, M. Rockelé, A. Chasin, D. Pham, J. Steiger, S. Botnaras, D. Weber, B. Herold, J. Ficker, B. van der Putten, G. H. Gelinck, J. Genoe, W. Dehaene, and P. Heremans, "Bidirectional communication in an hf hybrid organic/solution-processed metal-oxide rfid tag," *IEEE Transactions on Electron Devices*, vol. 61, no. 7, pp. 2387–2393, Jul. 2014.

[140] E. Cantatore, T. C. T. Geuns, A. F. A. Gruijthuijsen, G. H. Gelinck, S. Drews, and D. M. de Leeuw, "A 13.56mhz rfid system based on organic transponders," in *2006 IEEE International Solid State Circuits Conference - Digest of Technical Papers*, Feb. 2006, pp. 1042–1051.